MAT JOURNALS
Journal of Remote Sensing GIS & Technology
Volume 4 Issue 3

Method for Forecasting of Changes in Land Use and Land Cover Using Satellite Remote Sensing Techniques

[1]Dr. Adriana Márquez Romance, [2]Dr. Edilberto Guevara Pérez, [3]Dr. Demetrio Rey Lago
[1, 2]Professor,
Center of Hydrological and Environmental Research, University of Carabobo, Venezuela
[3]Professor,
Institute of Mathematics and Compute Applied, University of Carabobo, Venezuela

Abstract

In this investigation is proposed a method for forecasting of changes in land use and land cover using satellite remote sensing techniques. This study includes thefollowing twelve stages: 1) acquisition of remote sensing data, 2) collection of the reflectance image time series, 3) preliminary processing of reflectance image time series, 4) transformation of reflectance image to principal components, 5) modelling of PC1 statistical spatial prediction, 6) calibration of forecasting models for the PC1 SSPM coefficients, 7) calibration of PC1 SSPM, 8) validation of PC1 SSPM, 9) forecasting of PC1 SSPM coefficients and 10) calibration of CP1 SSPM with forecasted coefficients, 11) application of change detection techniques and 12) comparison of methods. Sixteensatellite images are acquired from the Landsat satellite in the period from 1986 to 2016. The study unit is the Pao river basin. The proposed method is a hybrid combination that includes three types of applied models that are based on time series of reflectance images in sequence as follows: the principal component analysis, the statistical spatial prediction models and forecasting models for time series. The current study proposes a method that contributes to introduce the temporal pattern of LULC changes captured by the statistical spatial prediction method coefficients and provides results characterized by a seasonality parameter; which is able to reproduce the spatio-temporal variation collected by the reception of the reflectance variable by satellite sensor. The statistics of error predictions indicate gradients of the predicted and observed function approximated to the unity as well as near to zero for the errors. The samples evaluated in the validation stage give correlation coefficient upper to 0.6; being a successful adjust between observed and predicted values. The forecasted changes in the Pao river basin for 2020 and 20130 vary from: 5.54 to 8. 14%, 5.52 to 8. 14%. These changes are equivalent to those observed from 2000 and 2016 of 5.13% as well as from 1990 to 2016 of 7.05 %.

Keywords: *LULC changes forecasting method, remote sensing, Land Use/Land Cover, Change detection techniques*

INTRODUCTION

The term land use refers to how the land is being used by human beings. Land cover refers to the biophysical materials found on the land (Jensen, 2009). Land use and land cover (LULC) changes may have an impact on the environment, ecosystem and socio-economic development in the region (Chen and Wang, 2010). In the environmental policy plans there is an increasing need for up-to-date and reliable information on land use and land cover environment (Stanners and Bourdeau 1995). This information is essential for planning and implementing policies to optimize the use of natural resources and accommodate development whilst minimizing the impact on the environment. The detection and monitoring of change in LULC using satellite multi-spectral image data has been supported on several techniques for accomplishing change detection have been formulated, applied and evaluated

(Dewidar, 2004). The change detection techniques are based on two discrete groups (Hussain et al., (2013); both of them using the image as unit of analysis. The first group uses the image pixel as fundamental unit of analysis, known as pixel-based. The second group is the object-based method, making image objects and then using them for further analysis. For example into the first group, the change vector technique has been applied by Thenkabail et al., (2005) to estimate the demand for water for irrigationin the Ganges and Indus river basins using 7-band MODIS land data for 2001–2002. Zhao et al., (2004) compare three techniques for change detection in order to select the best technique to manage cultivated areas and make a sustainable utilization: 1) image ratioing, 2) post-classification comparison and 3) Knowledge-based The techniques that involve the maximum likelihood algorithm to achieve the LULC classification and the post-classification comparison of images, are applied by the following researchers: Dewidar (2004) assess possible future changes following construction of the international coastal road, which crosses the study area located in the northern part of the Nile delta, Egypt, by analyzing the LULC changes between 1984 and 1997. Onur et al, (2009) take decision about two conflicting interests in Kemer, Turkey: agricultural production and tourism activity, by analyzing the LULC changes from 1975 to 2003. Chen and Wang, (2010) determine the environmental impacts by the drastic LULC changes experimented since the commencement of the construction of the Three Gorges Dam in 1994. In the second group, Bontemps et al, (2012) apply the object-based change detection algorithm to monitor land cover over large areas using SPOT-VEGETATION time series from 2000 to 2008. Regarding to the forecasting method, the highest frequency of application is the Markovian chains analysis (Jianping et al., 2005; Yin et al., 2007; Hadi et al., 2014; Kumar et al., 2014; Han et al., 2015; Padonou et al., 2017); which requires in order to generate the predictions at least two LUCL maps corresponding to date separated in time. A second applied method is based on neural networks focused in multi-layer perceptron with a low frequency (Pijanowski et al., 2002; Mishra et al., 2014). Both methods require a preview application of the supervised classification algorithms and post-classification comparison to obtain the LULC maps.

The land use and land cover (LULC) change detection methods are applied on the Pao river basin, Venezuela in order to find out the possible influence caused by these changes on the operation of the three reservoirs that provide water for residential-industrial-commercial uses in three states in the north-region of the country in the period from 1986 to 2016. The Pao river basin is a study unit that is composed by the following LULC: agricultural, rangeland, urban, water, vegetation and degraded soil (Figure 1). The LULC forecasting method proposed is compared with three methods based on pixels; which have been applied to determine LULC: 1) image difference (Nelson, 1983), 2) image ratioing (Howarth and Wickware, 1981), principal components (Byrne et al., 1980). In this study are included eleven images acquired from the Landsat satellite in the period between 1986 and 2016. The purpose is to create a method to forecast the LULC changes, finding the better approximation to the observed changes and predicting future changes in order to take decision to manage natural resources in a way that allowsto preserve its availability for the future human development.

STUDY SITE

The Bolivarian Republic of Venezuela is located in the American continent, north of

South America, in direct contact with the Caribbean Sea. It is located according to latitude in the northern hemisphere, between Ecuador and Tropic of Cancer, and according to the length in the Western hemisphere, with the following coordinates: 00°38'53" and 12°12´00" LN, 59°47´50" and 73°22´38" LW. The Paoriver basin is located in the central-north region of Venezuela.It covers a portion of area related to the total area of each of the three states as follows: Carabobo (1701.64 km^2, 4 866.75 km^2, 34.96%), Cojedes (1316.78 km^2, 13 878.24 km^2, 9.48%) and Guarico (0.123 km^2, 65 126.57 km^2, 0.0018 %).The total area of the Pao river basin is 3018.54 km^2; whose latitude and longitude varies between9°34' and 10°21', 67°46' and 68°15', respectively(Figure 1). The elevations of the Pao river basin vary from 1788 to 119 meters above sea level (masl). The elevations classified regarding to the occupied area in the Pao river basinare: 119 – 339 masl (777.08 km^2; 25.74%), 339.01 – 599 masl (1483.57 km^2; 49.14%), 599.01 – 962 masl (597.44 km^2, 19.79%) and 962.01 – 1 788 masl (160.43 km^2; 5.31%). This includes main river the fourteen identified as: 1) Chrigua, 2) Paito, 3) Cabriales, 4) PiraPira, 5) San Pedro, 6) Caiman, 7) Caimancito, 8) Pao, 9) Aragüita, 11) Mucaria, 12) Pacaragua, 13) Gamelotal and 14) Palmar. The three water reservoirs are located in the Pao river basin indicated according to the level of classification of the sub-basin as follows: a) Guataparo (upper sub-basin integrated by river: 2), b) PaoCachinche (intermediate sub-basin integrated by rivers : 1, 2, 3, 4 and 5) and c) Pao La Balsa (Lower sub-basin integrated by rivers: 7, 8, 9, 10, 11, 12, 13 and 14) (Figure 1).These water reservoirs are a source of water supplyfor the land use developed in the three states, whose urban population is as follows: 1) Cojedes (265 541 habitants), 2) Carabobo (2 208 188 habitants) and 3) Aragua (1 557 151 habitants) (Figure 1). The land cover / land use according to the U.S. Geological Survey Land-Use/ Land-Cover Classification System for use with remote sensor data (Anderson, 1976; Jensen, 2009) arefive mainly: 1) urban,2) agricultural, 3) rangeland, 4) forestland and 5) water. The terrain slopes and its corresponding area vary in the following intervals: 0 – 15% (1 581.76 km^2; 52.4%), 15 – 47% (1 058 km^2; 35.05%), > 47 % (378.56 km^2; 12.5%) (Figure 1).

METHODS

The method proposed for the forecasting of changes inLULCusing satellite remote sensing techniques is described in thefollowing the twelve stages (Figure 2): 1) acquisition of remote sensing data, 2) collection of the reflectance image time series, 3) preliminary processing of reflectance image time series, 4) transformation of reflectance image to principal components, 5) modelling of PC1 statistical spatial prediction, 6) calibration of forecasting models for the PC1 SSPM coefficients, 7) calibration of PC1 SSPM, 8) validation of PC1 SSPM, 9) forecasting of PC1 SSPM coefficients and 10) calibration of CP1 SSPM with forecasted coefficients, 11) application of change detection techniques and 12) comparison of method.

Acquisition of data

Acquisition of remote sensing data

The acquisition of remote sensing data is done from the following web site: https://earthexplorer.usgs.gov/; where the images from different satellites are available to access at no cost. The selected satellites are the group of Landsat satellites; using images from four of these: 1) Landsat 4 (L4), Landsat 5 (L5), Landsat 7 (L7) and Landsat 8 (L8); whose sensors are: L4 and L5: Thematic Mapper (TM), L7: Enhanced Thematic Mapper (ETM) and L8: Operational Land Imager (OLI); respectively. Sixteen Landsat images have

been acquiredcorresponding to a single scene; where the Pao river basin is contained. The scene is identified under the world reference system according to the following raw and path: 005, 053, respectively. These images represent the LULC condition mainly during the dry season; which covers the months between December and March of each year. The temporal series of images from the four Landsat satellite can be grouped as follows: 1) L4TM (1987, 1988, and 1989), 2) L5TM (1986, 1990, 1991, 1996, 1997, 1998, 1999and 2001), 3) L7ETM (2000, 2002, and 2003) and 4) L8OLI (2015, 2016).The parameters of map projection according to the United State Geological Survey (USGS) are: a) Projection: Universal Transverse Mercator (UTM), b) Datum: World Geodetic System 1984 (WGS84), c) UTM Zone: 19 N and e) Resample Method: Cubic Convolution. The image characteristics acquired according to each satellite are identified as follows (Table 1): a) the scene identification code, b) the acquisition date, c) the scene center time, d) the cloud coverage, e) the image quality, f) the angle of solar azimuth and g) the angle of solar zenith. In the Table 1, these can be observed as follows: LT50050531986351XXX03; 1986-12-17; 14: 11: 28.3900750Z; 20.00%; 7; 134.93319530 °; and 42.24871979 °.The criteria for selecting of the temporal series of Landsat images are: 1) the same season of each year, and 2) the lowest coverage of: clouds, aerosols and haze. The clouds and their associated shadows, aerosols and haze obstruct the ground view; causing atypical values in the reflectance observations through time. This can lead to confusion of the LULC change detection and the analysis of the reflectance trends. The dependence of the cloud free images restricts the sampling opportunities to the dry season in the tropics (Sano et al., 2007). Images affected by clouds, aerosols and haze often contain a large number of free pixels that can be used.

Collection of the imagetime series

The available Landsat satellite imageswere collected in order to make the largest amount and the longest time series. Two time series have been achieved by taking the images from the dry season of each year during the period between 1986 and 2003; whose seasonality is approximately one year. The two time series (TS)include the images of the following periods: First TS: from 1986 to1991, Second TSfrom 1996 to 2003. These two time series will be used to develop the forecast models for each one.

Preliminary processing of image time series

The preprocessing of the Landsat satellite data implies to apply the following absolute and relative corrections: geometric, radiometric, topographic and atmospheric. The correction algorithm application requires the band composition of each image using the ArcGIS V10.0 computational tool. The spectral bands included in the composition depend on each Landsat satellite as it is indicated in Table 3; where it can be seen as an example that the spectral bands included in the Landsat 5TM vary in the solar and thermalreflective regions as follows: spectral band 1 (b1): 0.452-0.518 µm. spectral band 2 (b2): 0.528-0.609 µm. spectral band 3 (b3): 0.626-0.693 µm. spectral band 4 (b4): 0.776-0.904 µm. spectral band 5 (b5): 0.776-0.904 µm. spectral band 6 (b6): 10.45-12.42 µm. spectral band 7 (b7): 2.097-2.349 µm.There are differences in the range of the spectral bandsbetween the Landsat 5TM and Landsat 7ETM satellites regarding to Landsat 8OLI satellite. The composite bands of each image according to each satellite are (Table 3): L5TM (b1, b2, b3, b4, b5, b7), L7ETM (b1, b2, b3, b4, b5, b7) and L8OLI (b2, b3, b4, b5, b6, b7); excluding those spectral bands into the thermal region.

Transformation of reflectance image tothe principal components (PC)

The reflectance image is transformed to the principal components (PC), mathematically based on ‘‘Principal Axis Transformation”. Principal components analysis (PCA) is a statistical technique that transforms a multivariate data set consisting of intercorrelated variables into a data set consisting of variables that are uncorrelated linear combinations of the original variables(Lillesand et al.,2014). The transformed variables are referred to as principal components (PCs). PCs are chosen in such a way that the first PC expresses the maximum possible proportion of the variance in the original data set; subsequent PCs account for successively smaller proportions of the remaining variance (Ingebritsen and Lyon, 1985). In this study, the first principal component (PC1) is selected as the image that will be used to obtain the statistical spatial prediction model.

Modelling of PC1 Statistical Spatial Prediction

It will be applied models of statistical spatial prediction for estimating of the PC1. A spatial prediction model (SSPM) estimates the values of the target variable (z) at some new location s_0; being a set of observations of a target variable z denoted as $z(s_1)$, $z(s_2)$,. . . , $z(s_n)$, where $s_i = (x_i, y_i)$ is a location and x_i and y_i are the coordinates (primary locations) in geographical space and n is the number of observations. The geographical domain of interest (area, land surface, object) can be denoted as A. It defines inputs, outputsand the computational procedure to derive outputs based on the given inputs (Hengl, 2007):

$\hat{z}(s_0) = E\{Z/z(s_i), q_k(s_0), \gamma(h), s \epsilon A\}$

Where $z(s_i)$is the input point dataset, $q_k(s_0)$is the list of deterministic predictors and $\gamma(h)$ is the covariance model defining the spatial autocorrelation structure. The type of SSPM used is the statistical model called Ordinary Krigging (OK); whose technique was developed by Krige (1951). The predictions are based on the model:

$Z(s) = \mu + \varepsilon'(s)$(1)

Where μ is the constant stationary function (global mean) and $\varepsilon'(s)$is the spatially correlated stochastic part of variation. The predictions are made as in

Matheron (1963) and Gandin (1960) introduced to the analysis of point data is the derivation and plotting of the so-called semivariances — differences between the neighbouring values:

$\gamma(h) = \frac{1}{2} E\left[\left(z(s_i) - z(s_i + h)\right)^2\right]$(2)

where z(si) is the value of target variable at some sampled location and z(si +h) is the value of the neighbour at distance si + h. The semivariances versus their distances produce a standard experimental variogram. From the experimental variogram, it can be fitted using some of the authorized variogram models, such as linear, spherical, exponential, circular, Gaussian, Bessel, power and similar (Isaaks and Srivastava, 1989; Goovaerts, 1997).

Forecasting of PC1 SSPM Coefficients

The forecasting of PC1 SSPM coefficients is made using the models provided to forecast the future values; which include various types of exponential smoothers, trend models, and parametric models of type “AutoRegressive, Integrated, Moving Average “(ARIMA), among others; which can be consulted in Box et al., (1994) and Hamilton, (1994). Two time series of PC1 SSPM coefficients have been used to adjust two forecasting models. The first time series corresponding to the period between 1986 and 1991 is used to calibrate the forecasting models and generate the time series of theforecasted PC1 SSPM coefficients in the period between 1992 and 2003. The second time series corresponding to the period between 1996 and 2003 is used to calibrate the

forecasting models and generate the time series of the forecasted PC1 SSPM coefficients in the period between 2004 and 2017. The criterion to choose the time period to obtain the forecasted PC1 SSPM coefficients in each time series is to do a comparison between the forecasted CP1 and the observed CP1 maps.

Calibration of PC1 SSPM coefficients

The calibration of the PC1 SSPM coefficients involves the choice of the forecasting model, whose error statistics between the observed and forecasted data are the lowest. Once the forecasting model has been selected, the PC1 SSPM coefficients are estimated for a future time. The statistic errors included are: root mean squared error (RMSE), mean absolute error (MEA), mean error (ME). The forecasted PC1 SSPM coefficients are evaluated in the SSPM using the last CP1 image integrating the available time series as the independent variable, then the error predictions between the forecasted and observed data are extracted by the following statistics: PRF: Predicted Regression function, ERF: Error Regression Function, SERF: Standardized Error Regression Function, PE: Prediction Errors.

Validation of PC1 SSPM coefficients

The validation of forecasting of PC1 SSPM coefficientsgenerated fromeach time series comprised between 1986 and 1991; as well as 1996 and 2003 is carried out by comparing a sample of values extracted from the forecasted PC1 map with a sample of values extracted from the observed PC1 map. The observed PC1 map is obtained from the reflectance image acquired by the Landsat satellite. The observed periods for the validation of the forecasted results from the first and second series comprises between 1996 and 2003, 2015 and 2016, respectively. The statistics that show the validation are: predicted regression function (PRF), correlation coefficient (CC), Determination Coefficient (R^2), Adjusted Determination Coefficient (R^2adjusted), Standard Error of Estimation (SEE), Mean Absolute Error (MAE), Durbin-Watson statistic (DW).

Application of Change Detection Techniques

The change detection techniques belong to two groups (Hussain et al., 2013): 1) pixel-based and, 2) object-based. The methods applied in this study corresponding to the first group: 1) Direct comparison: image differencing and image ratioing, 2) Transformation from image: principal components analysis.

Comparison of Results with Conventional Techniques

The comparison of results is carried out between the methods of change detection to estimate the grade in which the forecasted PC1 predicts the changes theLULC classes in the Pao river basin.

RESULTS

Results of application of the transformation method of principal components (PC)

The results of application of the transformation method of principal components expressed by the covariance matrix from the reflectance percentage image ofthe Pao river basin for 1986 are shown in the Table 3; where it can be observed that the covariance vectors of the principal components (PCs) are similar in the following two groups: First group: PC1, PC2 and PC3 and the Second group: PC4, PC5 and PC6.

The results of transformation method of principal components expressed by the correlation matrix from the reflectance percentage in the Pao river basin image for1986 are shown in the Table 4; where it can be observed that the correlation vectors of the principal components (PC)

are similar in the following two groups: First group: PC1, PC2 and PC3 and the Second group: PC4, PC5 and PC6.In the first group of PCs, the highest correlation corresponds to the spectral bands in the optical region varying between 0.96 and 1, the spectral bands in the infrared region are correlated with PCs varying from 0.65 to 0.86. Regarding to the second group of PCs, the correlation in the spectral bands in the optical region varies between 0.65 and 0.91, the highest correlation in found in the spectral bands of the infrared region varying from 0.76 to 1.

The results of transformation method of principal components expressed by the eigenvalues from the reflectance percentage images between 1986 and 2016 in the Pao river basin are shown in Table 5; where it can be observed that the variance of each PCs expressed as the eigenvalues takes the highest value in the PC1 by comparing with the rest of the PCs; which represents the greatest part of total population variance varying between 80.63 and 91.94%. As a sample, the eigenvalues and the percentage of variance in the PCs correspond to the reflectance image for 1986 are indicated as follows: PC1: 462.42, 87.1; PC2: 48.56, 9.15%; PC3: 17.24, 3.25%, PC4: 1.28, 0.24%, PC5: 1.13, 0.21% and PC6: 0.27, 0.05%, respectively. As a consequence, the PC1 is selected as the image to apply the modelling of statistical spatial prediction.

Results of the modelling of PC1 Statistical Spatial Prediction

The results of the modelling of PC1 statistical spatial prediction for the time series of images between: 1986 and 1991, 1996 and 2003, 2015 and 2016 are shown in Tables 6, 7 and 8, respectively. In general, the variogram of each PC1 image have been adjusted to a number of lags equal to 5. The statistical spatial prediction model (SSPM) selected in all cases is the J-Bessel function. The components or coefficients of the SSPM expressed in the Tables 6, 7 and 8 by the general equation a*Nugget+b*J-Bessel(c, d) are identified as follows: 1) a: the nugget, 2) b: the partial sill, 3) c: the range, and 4) d: the parameter. As a sample, in the image of date: 1986-12-17, the CP1 SSPM is described by: 159.64*Nugget+31.758*J-Bessel (7602, 5.7902); being the coefficients: a: 159.64, b: 31.758, c: 7602 and d: 5.7902. The gradients of the followinglinear functions vary between: predicted regression (PRF): 0.696 and 0.911, error regression (ERF): -0.088 and -0.303, standardized error regression (SERF): -0.00586 and -0.052. The sample size is: 3209460. The error predictions varying between: 1) Mean Error: -0.000305 and 0.00184, 2) Root-Mean-Square Error: 3.766 and 7.420, 3) Mean Standardized Error: -7.85e-005 and 0.000225, 4) Root-Mean-Square Standardized Error: 0.4005 and 0.818, 5) Average Standard Error: 5.568 and 18.052.

Results of calibration of forecasting models for the PC1 SSPM Coefficients

The results of calibration of forecasting models for the PC1 SSPM Coefficients based on the time series between 1986 and 1991, 1996 and 2003 are shown in Tables 9 and 10; where it can be observed that the five models included for the forecasting of the four coefficients are: 1) ARIMA, 2) Linear Trend, 3) Simple exponential smoothing, 4) Brown's linear exponential smoothing, and 5) Brown's quadratic exponential smoothing. In general, the ARIMA model is represented by the parameters: (1,0,0) with constant; where the order of the no seasonal autoregressive term is equal to 1, the order of the no seasonal differencing is of zero, and the order of the no seasonal moving average term is of zero.

Results of the error statistics by fitting the forecasting models to the PC1 SSPM coefficients

The error statistics by fitting the forecasting models to the PC1 SSPM coefficients based on the two time series between 1986 and 1991, and 1996 and 2003 are shown in Tables 11 and 12; where it can be observed the three following error statistics: 1) RMSE: root mean squared error, 2) MAE: mean absolute error and 3) ME: mean error. In general, the four coefficients are estimated with the lower error by the A model corresponding to the ARIMA Model: (1,0,0) with constant. In the first time series, a: RMSE: 43.0168, MAE: 26.4774, ME:3.2464; b: RMSE: 149.069, MAE: 104.798, ME:4.349; c: RMSE: 4306.73, MAE: 3113.61, ME:189.467; d: RMSE: 3.84892, MAE: 2.67851, ME:-0.0371282. In the second time series, a: RMSE: 71.3372, MAE: 46.1758, ME:-2.03837E-12; b: RMSE: 174.613, MAE: 85.5275, ME:-38.578; c: RMSE: 7411.07, MAE: 4401.36, ME:-18.0989; d: RMSE: **01972, MAE: 2.94246, ME:0.0740119.**

The two time series of the forecasted PC1 SSPM coefficients from 1992 to 2030; and from 2004 to 2030 based on the two time series from 1986 to 1991, as well as from 1996 to2003,respectively,are obtained through of the selected forecast models from the Tables 11 and 12.These forecasted coefficients are shown in Tables 13 and 14. In the first and second time series, the ARIMA(1,0,0)and Brown's linear exponential smoothing models are used to forecast the four coefficients associated to the PC1 SSPM, respectively. As an example, in the first time series, the forecasted PC1 SSPM coefficients for 1996 are: a: 74.4782, b: 121.29, c: 3464.67 and d:6.45658.In the second time series, the forecasted PC1 SSPM coefficients for 2016 are: a: 108.75, b: 151.703, c: 3774.29 and d:7.77191.

Results of the calibration of the PC1 SSPM

The calibration of the PC1 SSPM with forecasted coefficients between 1996 and 2003 are obtained based on the time series between 1986 and 1991 and indicated in Table 15. In addition, it is included the calibration of the PC1 SSPM corresponding to 2016. The coefficients are applied using as independent variable to the PC1 image last in the time series corresponding to 1991. The statistical spatial prediction model (SSPM) selected in all cases is the J-Bessel function. The components or coefficients of the SSPM expressed in the Table 15 by the general equation a*Nugget+b*J-Bessel(c, d) are identified as follows: 1) a: the nugget, 2) b: the partial sill, 3) c: the range, and 4) d: the parameter. As a sample, in the image of 1996, the CP1 SSPM is described by: 74.478*Nugget+121.29*J-Bessel(3464.7,6.4566)); being the coefficients: a: 74.478, b: 121.29, c: 3464.7 and d: 6.4566. The forecasted gradients of the following linear functions vary as follows: predicted regression (PRF): 0.7824, error regression (ERF): -0.2175, standardized error regression (SERF): -0.0263. The sample size is: 3209460. The error predictions vary in the following ranges: 1) Mean Error: -0.00147 and -0.000184, 2) Root-Mean-Square Error: 4.834 and 4.836, 3) Mean Standardized Error: -0.000174 and -0.0001828, 4) Root-Mean-Square Standardized Error: 0.546 and 0.603, 5) Average Standard Error: 8.0106 and 8.843.

The calibration of the PC1 SSPM with forecasted coefficients between 2015 and 2016 are obtained based on the time series between 1996 and 2003 and indicated in Table 16. The coefficients are applied using as independent variable to the PC1 image last in the time series corresponding to 2003. The statistical spatial prediction model (SSPM) selected in all cases is the J-Bessel function. The components or coefficients of the SSPM expressed in the Table 16 by the general equation a*Nugget+b*J-Bessel(c, d) are identified as follows: 1) a: the nugget, 2) b: the

partial sill, 3) c: the range, and 4) d: the parameter. As a sample, in the image of date: 2016-01-18, the CP1 SSPM is described by: 108.11*Nugget+157.31*J-Bessel (3791.7, 7.7866); being the coefficients: a: 108.11, b: 157.31, c: 3791.7 and d: 7.7866. The forecasted gradients of the following linear functions vary as follows: predicted regression (PRF): 0.8099, error regression (ERF): -0.19003, standardized error regression (SERF): -0.01793. The sample size is: 3209460. The error predictions varying between: 1) Mean Error: 0.000883, 2) Root-Mean-Square Error:3.770, 3) Mean Standardized Error: 8.1318e-005, 4) Root-Mean-Square Standardized Error: 0.3557, 5) Average Standard Error: 10.6550.

Results of the validation of PC1 SSPM

The validation of PC1 SSPM is obtained by comparing the estimated and observed PC1 between 1996 and 2003 based on the time series between 1986 and 1991 is shown in Table 17. As a sample, for the estimated PC1of 1996, the linear function between the predicted and observed is: 23.1465 + 0.423927*x; where x is the observed value. The statistics of the adjusted linear model are: Samples: 73, correlation coefficient (CC): 0.652297, determination coefficient: R^2: 0.425, adjusted determination coefficient: $R^2_{adjusted}$:0.4175, Standard Error of Estimation (SEE): 33.1997, Mean absolute error (MAE): 27.5367, and Durbin Watson Coefficient (DW): 1.14484. In general, the statistics vary between: CC: 0.566 and 0.6502, R^2: 0.3207 and 0.4254, $R^2_{adjusted}$: 0.3673 and 0.4175. SEE: 14.8382 and 33.1997. MAE: 12.7754 and 27.5367. DW: 0.892394 and 1.22745.

The validation of PC1 SSPM is obtained by comparing the estimated and observed PC1 between 2015 and 2016 based on the time series between 1996 and 2003is shown in Table 18. As a sample, for the estimated PC1 of 2016, the linear function between the predicted and observed is: 8.02645 + 0.422091*x; where x is the observed value. The statistics of the adjusted linear model are: Samples: 361, correlation coefficient (CC): 0.547798, determination coefficient: R^2: 0.300, adjusted determination coefficient: $R^2_{adjusted}$:0.2971, Standard Error of Estimation (SEE): 2.90821, Mean absolute error (MAE): 1.86529, and Durbin Watson Coefficient (DW): 1.25292.

Results of the forecasting of PC1 SSPM coefficients

The results of the forecasting for the two time series of PC1 SSPM coefficients from 1992 to 2030; from 2004 to 2030 based on the time series between 1986 and 1991, as well as 1996 and 2003, respectively, are shown in Tables 9 and 10 as it has been described in the section 4.3; these coefficients are generated from the ARIMA (1,0,0) and Brown's linear exponential smoothing models, respectively. As a sample, the forecasted PC1 SSPM coefficients for 2020 and 2030 are: First time series: 2020: a: 67.3352, b: 121.382, c: 3384.75, d: 6.48529. 2030: a: 67.2386, b: 121.382, c: 3384.75, d: 6.48529. Second time series: 2020: a: 110.164, b: 159.103, c: 3861.34, d: 7.66497. 2030: a: 122.366, b: 186.173, c: 4063.95, d: 7.326.

Results of the calibration of CP1 SSPM with forecasted coefficients

The results of the calibration of PC1 SSPM for 2020 and 2030 with forecasted coefficients based on the time series between 1986 and 1991, as well as 1996 and 2003 are shown in Tables 19 and 20. As a sample, for the estimated PC1of 2020 in the first time series, the CP1 SSPM is described by: 67.335*Nugget+121.38*J-Bessel (3384.8, 6.4853) being the coefficients: a: 67.335, b: 121.38, c: 3384.8and d: 6.4853. The predicted regression function (PRF): 0.782482497946622 * x +

8.66482580355468, error regression function (ERF): -0.217517502057148 * x + 8.66482580370286, standardized error regression function (SERF): -0.0258635513022785 * x + 1.03028148988674. The sample size is: 3209460. The error predictions vary in the following ranges: 1) Mean Error: -0.001485, 2) Root-Mean-Square Error: 4.83535, 3) Mean Standardized Error: -0.000179, 4) Root-Mean-Square Standardized Error: 0.57487, 5) Average Standard Error: 8.40924.

Results of the application of the change detection techniques

The results by applying the change detection technique based on the CP1 image difference corresponding to the bitemporal reflectance images as a proportion of Change / No Change areas in thePao river basin from 1986-2016 for the following cases: 1)using the forecasted PC1 image of 2016 from time series between 1986 and 1991 (Table 21 and Figure 3), 2) using the forecasted PC1 image of 2016 from time series between 1996 and 2003 (Table 22 and Figure 4), 3) using the original PC1 2016 (Table 23 and Figure 5).As a sample, the Change/No Change area for the 2015-2016 difference image is according to the cases:1)5.85 % and 94.14%, 2) 4.71 % and 95.28%, and 3) 3.98 % and 96.01%.In general, the Figures 3a and 3c, 4a and 4c, 5a and 5c show that the most of the changes occurs in the a and c water reservoirs and these are negatives,which means that the reflectance for 2016 is higher than in 1986 and 2000, respectively. The Figures 3b and 3d, 4b and 4d, 5b and 5d show that the most of the changes occurs in the urban zones and these are positives meaning that the reflectance for 2016 is lower than 1990 and 2015, respectively. The changes occur due to the transformation possible from vegetation to urban zones.

The results by applying the following methods expressed by the proportion of Change / No Change areas in the Pao river basin from 1986 to 2016; using the original PC1 images: a) difference of bitemporal reflectance images (Table 24), b) ratio of the bitemporal reflectance images (Table 25). As a sample, the Change/No Change area for the 2015-2016 is: a) 5.46 % and 94.54; b) 0.86 % and 99.14%, respectively.

Results of comparison of the change detection techniques

The results by comparing the change detection techniques are identified as follows (Figure 6): M1: PC1 image using the forecasted PC1 image of 2016 from time series between 1986 and 1991. M2: PC1 image difference using the forecasted PC1 image of 2016 from time series between 1996 and 2003. M3: using the original PC1 2016, M4: reflectance image difference, M5: image ratioing. The percentage in the areas of change / no change does not differ in a way significantly between the methods for 2000 and 2015. This is a validation mode of the results founded by the observed relative comparing in the description of the Figures 3, 4 and 5.

DISCUSSION

The proposed method is a hybrid that includes three types of applied models that are based on time series of reflectance images in sequence as follows: the principal component analysis, the statistical spatial prediction models and forecasting models for time series.

The forecasted results are shown by two future times and following cases (Figures 7 and 8, Tables 26, 27 and 28): 1) difference CP1 image being the forecasted CP1 based on the time series between 1986 and 1991: a) 2020-2016, b) 2030-2016 and 2) difference CP1 image being the forecasted CP1 based on the time series between 1986 and 1991: a) 2020-

2016, b) 2030-2016. In general, the pattern shown predicts two changes: 1) increase in the reflectance in the urban zone to the north of Pao river basin, this implies coverage extensions due to the urban grow; 2) decrease in the reflectance on the c water reservoir indicating a possible elimination of sediments and algae. The forecasted changes in the Pao river basin for 2020 and 20130 vary from: 5.54 to 8. 14% (Table 26, Figure 7), 5.52 to 8. 14% (Table 27, Figure 8). These changes are equivalent to those observed from 2000 and 2016 of 5.13% (Table 23) as well as from 1990 to 2016 of 7.05 % (Table 23).

The comparison of the forecasting methods of LULC change detection indicates the following aspects: 1) the method with the highest frequency of application is the Markovian chains analysis (Jianping et al., 2005; Yin et al., 2007;Hadi et al., 2014;Kumar et al., 2014; Han et al., 2015; Padonou et al., 2017); which requires in order to generate the predictions at least two LUCL maps corresponding to date separated in time, and to make a validation of results. The studies founded are recorded from the beginning of the year 2000 to the present. 2) In addition, another applied method is based on neural networks focused in multi-layer perceptron with a low frequency (Pijanowski et al., 2002; Mishra et al., 2014). Both methods require a preview application of the supervised classification algorithms and post-classification comparison to obtain the LULC maps. The current study proposes a method that contributes to introduce the temporal pattern of LULC changes captured by the statistical spatial prediction method coefficients and provides results characterized by a seasonality parameter; which is able to reproduce the spatio-temporal variation collected by the reception of the reflectance variable by satellite sensor.

CONCLUSIONS

The proposed method is a hybrid combination that includes three types of applied models that are based on time series of reflectance images in sequence as follows: the principal component analysis, the statistical spatial prediction models and forecasting models for time series. The current study proposes a method that contributes to introduce the temporal pattern of LULC changes captured by the statistical spatial prediction method coefficients and provides results characterized by a seasonality parameter; which is able to reproduce the spatio-temporal variation collected by the reception of the reflectance variable by satellite sensor. The statistics of error predictions indicates gradients of the predicted and observed function approximated to the unity as well as near to zero for the errors. The samples evaluated in the validation stage give correlation coefficient upper to 0.6; being a successful adjust between observed and predicted values.

REFERENCES

1. Bontemps, S., Bogaert, P., Titeux, N., &Defourny, P. (2008). An object-based change detection method accounting for temporal dependences in time series with medium to coarse spatial resolution. Remote Sensing of Environment, 112(6), 3181-3191.
2. Box, G. E. P., Jenkins, G. M., and Reinsel G. C. (1994). Time Series Analysis: Forecasting and Control. 3rd ed. Englewood Cliffs, NJ: Prentice Hall, 1994.
3. Byrne, G. F., Crapper, P. F., & Mayo, K. K. (1980). Monitoring land-cover change by principal component analysis of multitemporal Landsat data. Remote sensing of Environment, 10(3), 175-184.
4. Chen, Z., & Wang, J. (2010). Land use and land cover change detection using

satellite remote sensing techniques in the mountainous Three Gorges Area, China. International Journal of Remote Sensing, 31(6), 1519-1542.
5. Dewidar, K. M. (2004). Detection of land use/land cover changes for the northern part of the Nile delta (Burullus region), Egypt. International journal of remote sensing, 25(20), 4079-4089.
6. Gandin, L.S., 1960. On optimal interpolation and extrapolation of meteorological fields. Trudy Main Geophys. Obs. 114, 75–89.
Hamilton, J. D. (1994). Time Series Analysis. Princeton, NJ: Princeton University Press.
7. Goovaerts, P., Webster, R., & Dubois, J. P. (1997). Assessing the risk of soil contamination in the Swiss Jura using indicator geostatistics. Environmental and ecological Statistics, 4(1), 49-64.
8. Hadi, S. J., Shafri, H. Z., &Mahir, M. D. (2014). Modelling LULC for the period 2010-2030 using GIS and Remote sensing: a case study of Tikrit, Iraq. In IOP conference series: earth and environmental science (Vol. 20, No. 1, p. 012053). IOP Publishing.
9. Han, H., Yang, C., & Song, J. (2015). Scenario simulation and the prediction of land use and land cover change in Beijing, China. Sustainability, 7(4), 4260-4279.
10. Hengl, T. (2009). A practical guide to geostatistical mapping (Vol. 52). Hengl.
11. Howarth, P. J., &Wickware, G. M. (1981). Procedures for change detection using Landsat digital data. International Journal of Remote Sensing, 2(3), 277-291.
12. Hussain, M., Chen, D., Cheng, A., Wei, H., & Stanley, D. (2013). Change detection from remotely sensed images: From pixel-based to object-based approaches. ISPRS Journal of Photogrammetry and Remote Sensing, 80, 91-106.
13. Isaaks, E. H., & Srivastava, M. R. (1989). Applied geostatistics (No. 551.72 ISA).
14. Ingebritsen, S. E., & Lyon, R. J. P. (1985). Principal components analysis of multitemporal image pairs. International 1135 Journal of Remote Sensing, 6(5), 687-696.
15. Jianping, L., Bai, Z., & Feng, G. (2005). RS-and-GIS-supported forecast of grassland degradation in southwest Songnen Plain by Markov model. Geo-spatial Information Science, 8(2), 104-109.
16. Kumar, S., Radhakrishnan, N., & Mathew, S. (2014). Land use change modelling using a Markov model and remote sensing. Geomatics, Natural Hazards and Risk, 5(2), 145-156.
17. Lillesand, T., Kiefer, R. W., &Chipman, J. (2014). Remote sensing and image interpretation. John Wiley & Sons.
18. Matheron, G. (1963). Principles of geostatistics. Economic Geology, 58, 1246–1266.
19. Mishra, V. N., Rai, P. K., & Mohan, K. (2014). Prediction of land use changes based on land change modeler (LCM) using remote sensing: a case study of Muzaffarpur (Bihar), India. Journal of the Geographical Institute" Jovan Cvijic", SASA, 64(1), 111-127.
20. Nelson, R. F. (1983). Detecting forest canopy change due to insect activity using Landsat MSS. Photogrammetric Engineering and Remote Sensing, 49(9), 1303-1314.
21. Onur, I., Maktav, D., Sari, M., & Kemal Sönmez, N. (2009). Change detection of land cover and land use using remote sensing and GIS: a case study in Kemer, Turkey. International Journal of Remote Sensing, 30(7), 1749-1757.
22. Padonou, E. A., Lykke, A. M., Bachmann, Y., Idohou, R., &Sinsin, B. (2017). Mapping changes in land use/land cover and prediction of future

extension of bowé in Benin, West Africa. Land Use Policy, 69, 85-92.
23. Pijanowski, B. C., Brown, D. G., Shellito, B. A., &Manik, G. A. (2002). Using neural networks and GIS to forecast land use changes: a land transformation model. Computers, environment and urban systems, 26(6), 553-575.
24. Sano, E. E., Ferreira, L. G., Asner, G. P., & Steinke, E. T. (2007). Spatial and temporal probabilities of obtaining cloud-free Landsat images over the Brazilian tropical savanna. International Journal of Remote Sensing, 28(12), 2739-2752.
25. Stanners, D., and Bourdeau, P. (editors), 1995, Europe's Environment: the Dobris assessment (Luxembourg: Publications of the European Communities), ISBN 92-826-5409-5.
26. Thenkabail, P. S., Schull, M., &Turral, H. (2005). Ganges and Indus river basin land use/land cover (LULC) and irrigated area mapping using continuous streams of MODIS data. Remote Sensing of Environment, 95(3), 317-341.
27. Yin, D., Chen, X., Yan, L., & Huang, Z. (2007, July). The research and realization of the land-use change forecasting model in development zones based on RS and GIS. In Geoscience and Remote Sensing Symposium, 2007. IGARSS 2007. IEEE International (pp. 3429-3432). IEEE.
28. Zhao, G. X., Lin, G., & Warner, T. (2004). Using Thematic Mapper data for change detection and sustainable use of 1221 cultivated land: a case study in the Yellow River delta, China. International Journal of Remote Sensing, 25(13), 2509-2522.

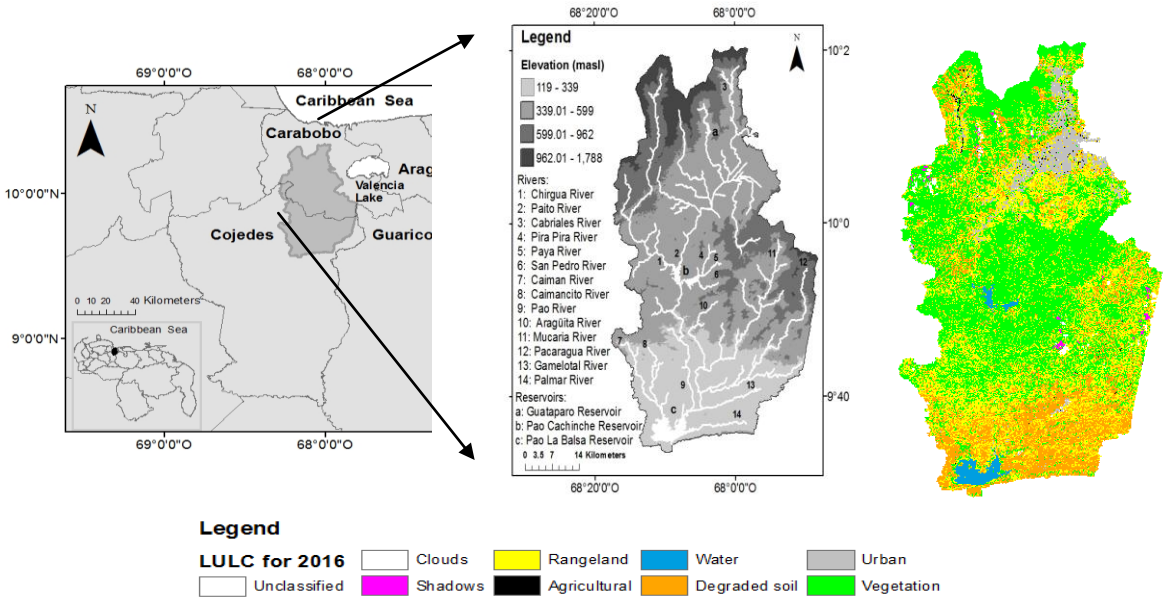

Fig 1. *Map of relative location of the Pao river basin regarding to the Bolivarian Republic of Venezuela. The study area is outlined in the box. The classified LULC map shows the spatial distribution of uses and coverage: 1) urban, 2) rangeland, 3) agricultural. 4) vegetation, 5)water reservoir, 6) clouds, and 7) shadows.*

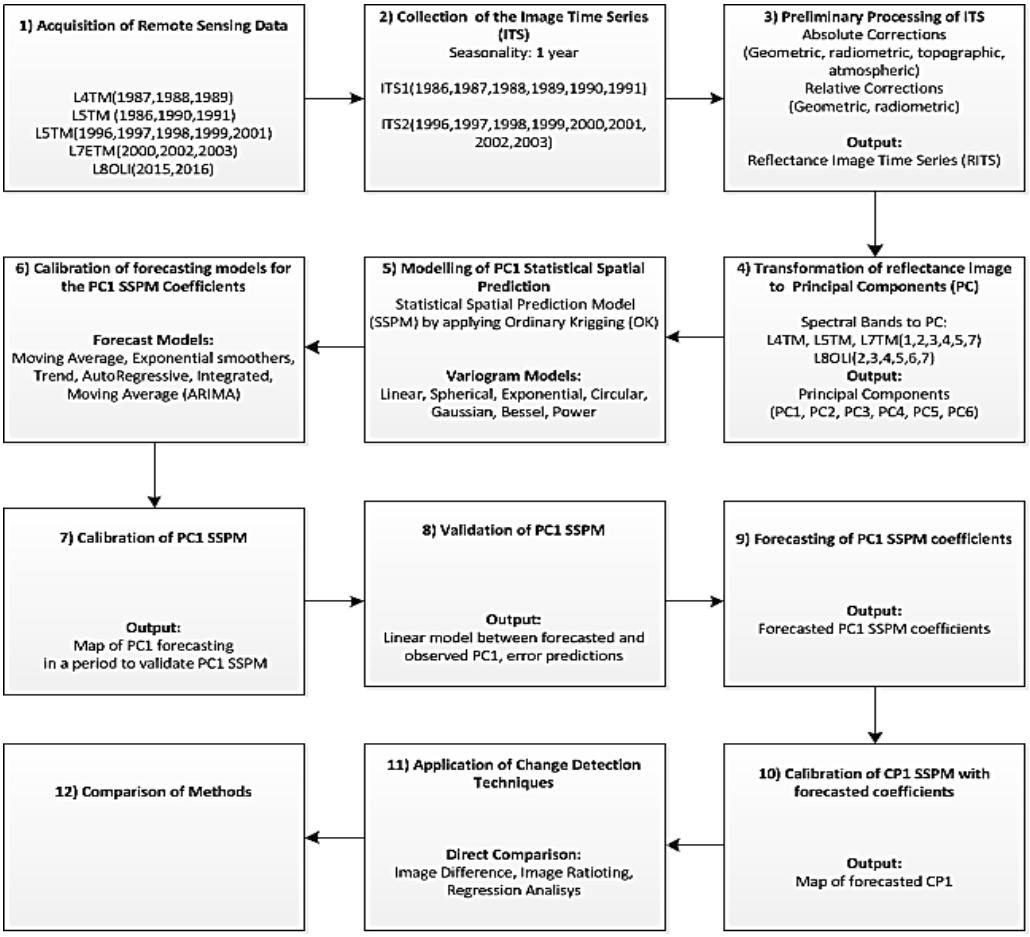

Fig 2. *Workflow of method for forecasting of changes in land use and land cover using satellite remote sensing techniques*

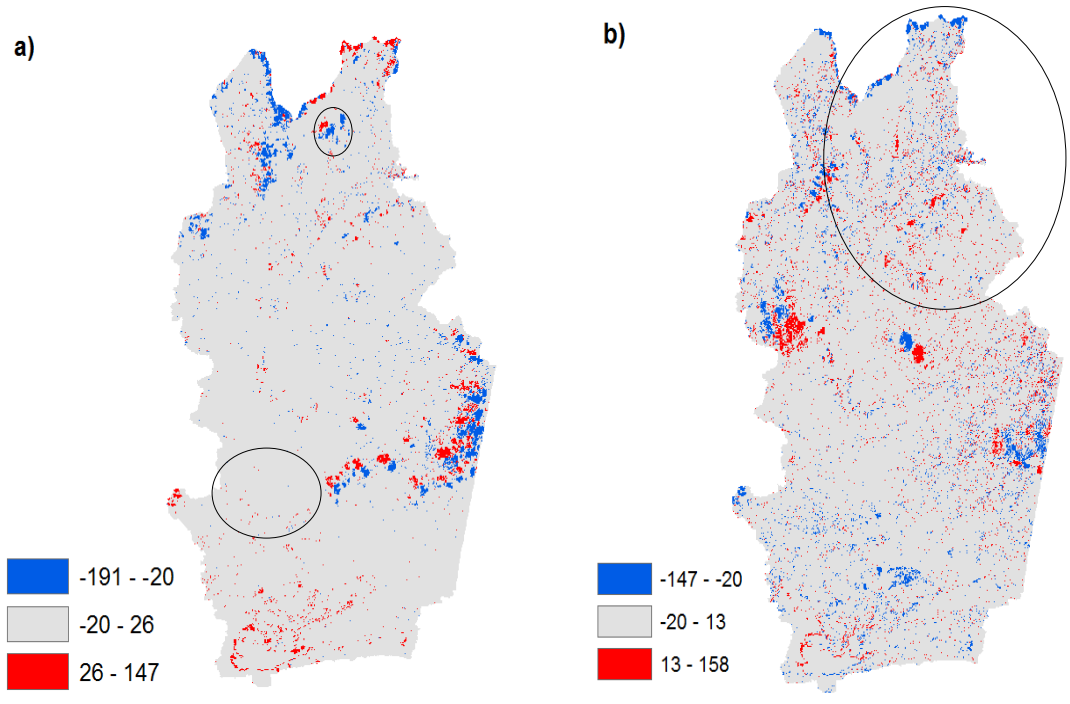

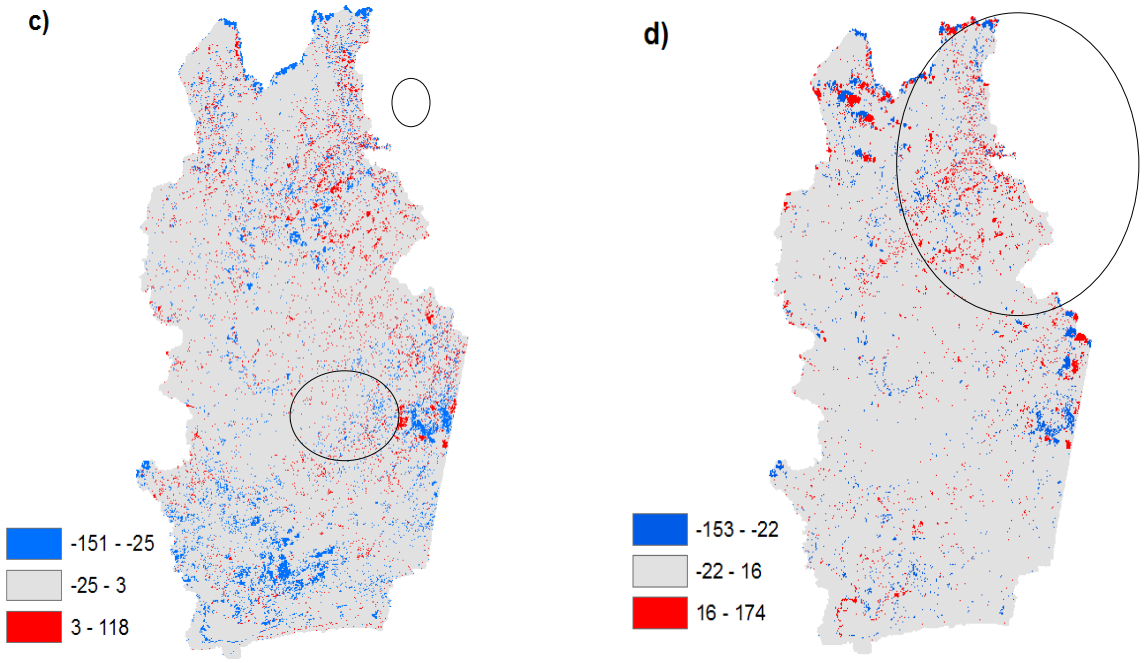

Fig 3. *Results by applying the change detection technique based on the difference of the principal component No. 1 corresponding to the reflectance images as a proportion of Change / No Change areas in the Pao river basin from 1986-2016; using the forecasted PC1 of 2016 from time series between 1986 and 1991. The parameters are: C: Change (Grey), NC: No Change (Blue/Red), PAR: Percentage Area Ratio. a) 1986-2016, b) 1990-2016, c) 2000-2016 and d) 2015-2016.*

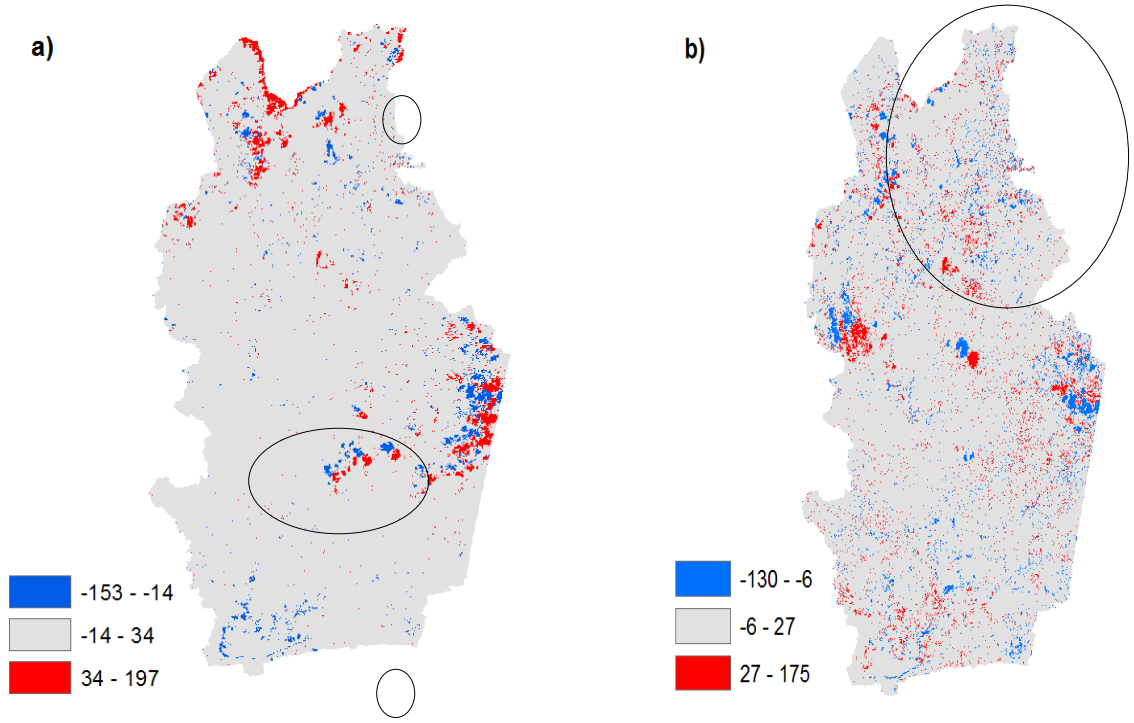

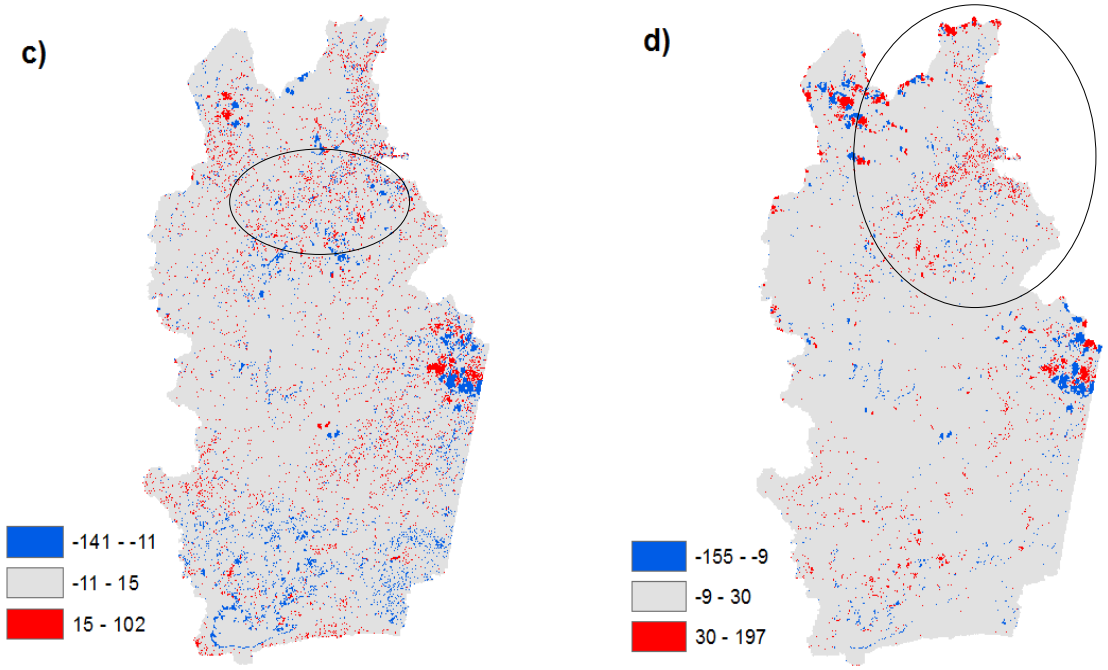

Fig 4. *Results by applying the change detection technique based on the difference of the principal component No. 1 corresponding to the reflectance images as a proportion of Change / No Change areas in the Pao river basin from 1986-2016; using the forecasted PC1 2016 from time series between 1996 and 2003. The parameters are: C: Change (Grey), NC: No Change (Blue/Red), PAR: Percentage Area Ratio. a) 1986-2016, b) 1990-2016, c) 2000-2016 and d) 2015-2016.*

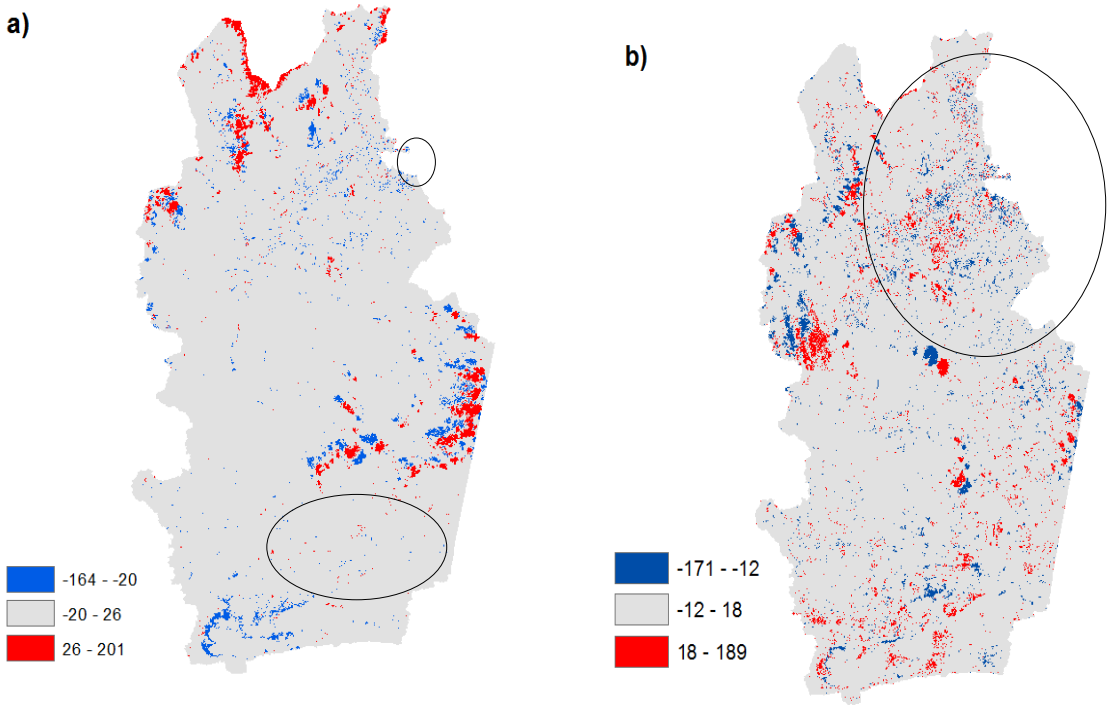

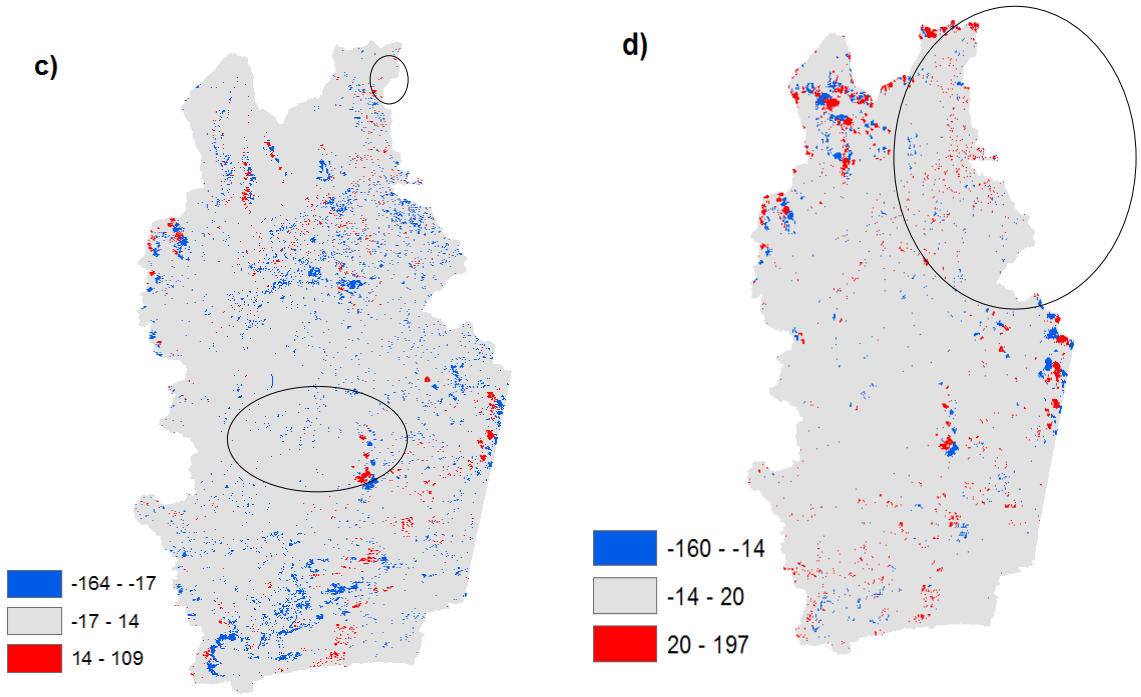

Fig 5. *Results by applying the change detection technique based on the difference of the principal component No. 1 corresponding to the bitemporal reflectance images as a proportion of Change / No Change areas in the Pao river basin from 1986-2016; using the observed PC1 of 2016. The parameters are: C: Change, NC: No Change, PAR: Percentage Area Ratio. a) 1986-1990, b) 1990-2016, c) 2000-2016 and d) 2015-2016.*

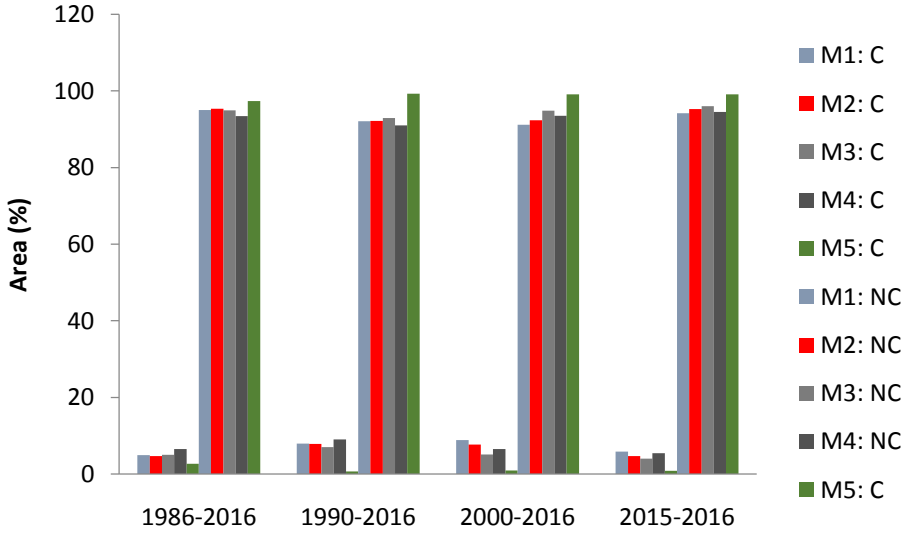

Fig 6. *Results by comparing the change detection techniques: M1: PC1 image difference using the forecasted PC1 image for 2016. M2: PC1 image difference using the observed PC1 image for 2016. M3: reflectance image difference, M4: image ratioing.*

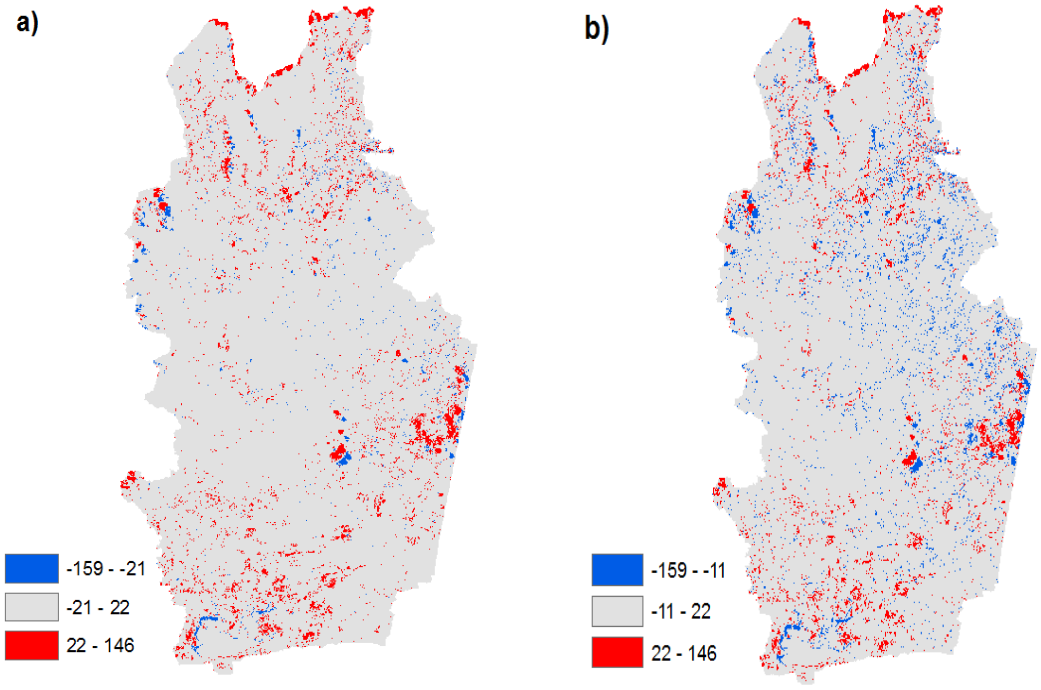

Fig 7. *Results of forecasted difference CP1 being the forecasted CP1 based on the time series between 1986 and 1991, a) 2020-2016, b)) 2030-2016*

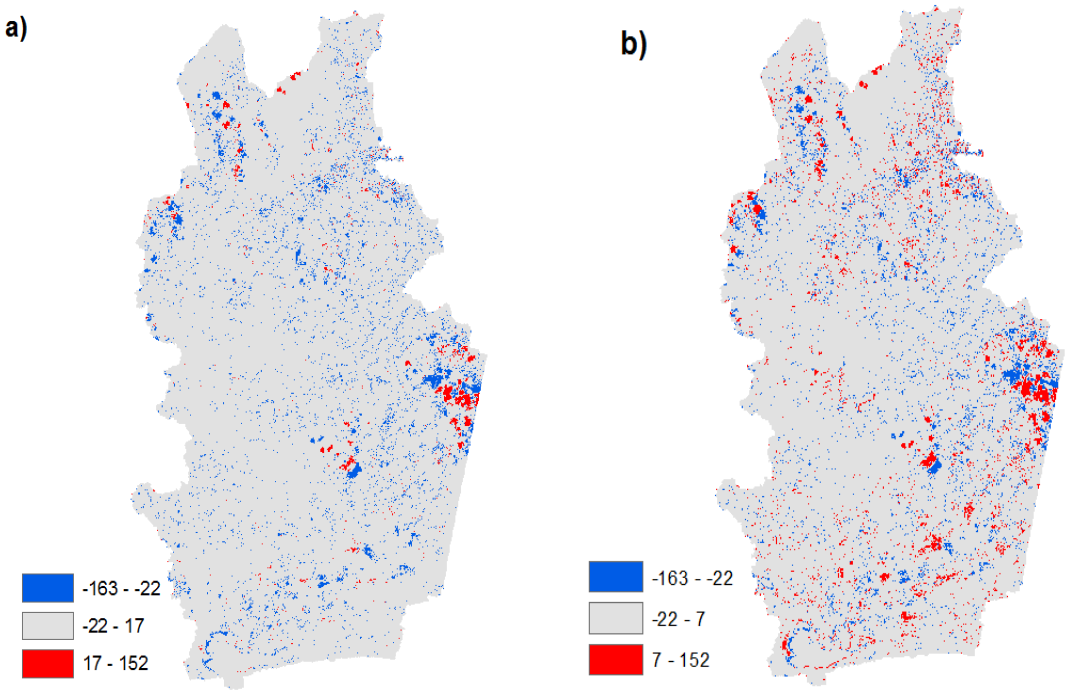

Fig 8.*Results of forecasted difference CP1 being the forecasted CP1 based on the time series between 1986 and 1991, a) 2020-2016, b)) 2030-2016*

Table 1 *Characteristics of Landsat satellite images corresponding to the 005, 053 scene containing the Pao river basin*

N°	1	2	3	4	5	6	7
1	LT50050531986351XXX03	1986-12-17	14:11:28.3900750Z	20.00	7	134.93319530	42.24871979
2	LT40050531987346XXX09	1987-12-12	14:14:44.6630060Z	15.00	9	135.91098925	43.53223353
3	LT40050531988093XXX01	1988-04-02	14:18:47.0440560Z	2.00	9	95.54851624	55.19353086
4	LT40050531989287XXX02	1989-10-14	14:25:49.9650380Z	27.00	9	121.81287211	56.05265489
5	LT50050531990010CPE03	1990-01-10	14:15:12.2020810Z	11.00	7	131.96692328	41.77289720
6	LT50050531991077CPE01	1991-03-18	14:14:04.6490630Z	28.00	7	104.58761331	51.37583561
7	LT50050531996299XXX02	1996-10-25	14:12:26.1290060Z	18.00	9	124.94450537	51.52871601
8	LT50050531997125AAA02	1997-05-05	14:20:38.5360810Z	50.00	9	75.28557916	57.71333274
9	LT50050531998032CPE00	1998-02-01	14:28:28.6110190Z	33.00	9	127.94531961	46.11991603
10	LT50050531999019CPE00	1999-01-19	14:31:37.3780560Z	23.00	9	132.94664692	45.23014868
11	LE70050532000014SGS01	2000-01-14	14:45:26.0198689Z	7.00	9	137.52485114	47.22916723
12	LT50050532001008AAA02	2001-01-08	14:32:22.5760750Z	10.00	9	135.84219087	44.77755780
13	LE70050532002051AGS00	2002-02-20	14:41:26.1414958Z	22.00	9	122.73905080	52.13911206
14	LE70050532003022PFS00	2003-01-22	14:41:05.9709036Z	10.00	9	134.07217263	47.15930857
15	LO80050532015063LGN00	2015-03-04	14:52:20.8148112Z	13.13	9	119.09567247	57.19634293
16	LC80050532016018LGN00	2016-01-18	14:52:41.9360648Z"	6.09	9	138.18721946	48.77317194

1) the scene identification code, 2) the acquisition date, 3) the scene center time, 4) the cloud coverage, 5) the image quality,6) the angle of solar azimuth and 7) the angle of solar zenith.

Table 2*Landsat Image Spectral Bands*

Landsat 4TM / 5 TM			Landsat 7 ETM			Landsat 8 OLI		
1 Unit	2 µm	3 m	1 Unit	2 µm	3 m	1 Unit	2 µm	3 m
Spectral Band 1	0.452-0.518	30	Spectral Band 1	0.452-0.514	30	Spectral Band 1	0.43 – 0.45	30
Spectral Band 2	0.528-0.609	30	Spectral Band 2	0.519-0.601	30	Spectral Band 2	0.45 – 0.51	30
Spectral Band 3	0.626-0.693	30	Spectral Band 3	0.631-0.692	30	Spectral Band 3	0.53 – 0.59	30
Spectral Band 4	0.776-0.904	30	Spectral Band 4	0.772-0.898	30	Spectral Band 4	0.64 – 0.67	30
Spectral Band 5	1.567-1.784	30	Spectral Band 5	1.547-1.748	30	Spectral Band 5	0.85 – 0.88	30
Spectral Band 6	10.45-12.42	30	Spectral Band 6	10.31-12.36	30	Spectral Band 6	1.57 – 1.65	30
Spectral Band 7	2.097-2.349	30	Spectral Band 7	2.065-2.346	30	Spectral Band 7	2.11 – 2.29	30

1: Spectral Band, 2: Spectral Range, 3: Cell Size

Table 3 *Results of transformation method of principal components expressed by the covariance matrix from the reflectance percentage image in 1986 in the Pao river basin*

	PC1	PC 2	PC 3	PC 4	PC 5	PC 6
Spectral Band 1	31.46	36.53	34.75	52.42	52.02	41.81
Spectral Band 2	36.53	44.75	42.31	69.37	67.38	52.04
Spectral Band 3	34.75	42.31	41.53	58.83	62.70	50.47
Spectral Band 4	52.42	69.37	58.83	191.36	149.65	90.79
Spectral Band 5	52.02	67.38	62.70	149.65	147.89	98.64
Spectral Band 7	41.81	52.04	50.47	90.79	98.64	73.90

Table 4 *Results of transformation method of principal components expressed by the correlation matrix from the reflectance percentage image in 1986 in the Pao river basin*

	PC1	PC 2	PC 3	PC 4	PC 5	PC 6
Spectral Band 1	1.00	0.97	0.96	0.67	0.76	0.86
Spectral Band 2	0.97	1.00	0.98	0.74	0.82	0.90
Spectral Band 3	0.96	0.98	1.00	0.65	0.80	0.91
Spectral Band 4	0.67	0.74	0.65	1.00	0.88	0.76
Spectral Band 5	0.76	0.82	0.80	0.88	1.00	0.94
Spectral Band 7	0.86	0.90	0.91	0.76	0.94	1.00

Table 5 *Results of transformation method of principal components expressed by the eigenvalues from the reflectance percentage images between 1986 and 2016 in the Pao river basin*

	Principal Components	PC1	PC 2	PC 3	PC 4	PC 5	PC 6
1986	Eigenvalues	462.42	48.56	17.24	1.28	1.13	0.27
	Percentage of Variance	87.1	9.15	3.25	0.24	0.21	0.05
1987	Eigenvalues	575.13	108.32	25.65	2.34	1.45	0.41
	Percentage of Variance	80.63	15.19	3.60	0.33	0.20	0.06
1988	Eigenvalues	923.04	51.47	21.88	5.33	1.69	0.49
	Percentage of Variance	91.94	5.13	2.18	0.53	0.17	0.05
1989	Eigenvalues	760.41	95.11	14.72	5.01	1.18	0.37
	Percentage of Variance	86.73	10.85	1.68	0.57	0.13	0.04
1990	Eigenvalues	381.68	40.11	8.42	1.16	0.69	0.21
	Percentage of Variance	88.30	9.28	1.95	0.27	0.16	0.05
1991	Eigenvalues	449.96	36.98	11.49	1.46	0.63	0.24
	Percentage of Variance	89.86	7.38	2.29	0.29	0.13	0.05
1996	Eigenvalues	975.80	158.89	16.82	6.11	1.53	0.41
	Percentage of Variance	84.15	13.70	1.45	0.53	0.13	0.04
1997	Eigenvalues	1,113.97	114.25	48.13	6.36	2.49	0.67
	Percentage of Variance	86.63	8.89	3.74	0.49	0.19	0.05
1998	Eigenvalues	374.23	28.7	7.53	1.22	0.58	0.19
	Percentage of Variance	90.73	6.96	1.83	0.30	0.14	0.05
1999	Eigenvalues	347.8	38.53	7.21	1.07	0.43	0.2
	Percentage of Variance	88.00	9.75	1.82	0.27	0.11	0.05
2000	Eigenvalues	228.58	22.2	6.41	0.85	0.28	0.13
	Percentage of Variance	88.44	8.59	2.48	0.33	0.11	0.05
2001	Eigenvalues	368.47	35.46	35.46	1.27	0.55	0.23
	Percentage of Variance	83.47	8.03	8.03	0.29	0.12	0.05
2002	Eigenvalues	270.95	17.73	6.28	0.87	0.43	0.16
	Percentage of Variance	91.41	5.98	2.12	0.29	0.14	0.05
2003	Eigenvalues	221.75	17.09	8.32	1.09	0.43	0.15
	Percentage of Variance	89.12	6.87	3.34	0.44	0.17	0.06
2015	Eigenvalues	417.51	42.73	22.53	1.14	0.84	1.14
	Percentage of Variance	85.93	8.79	4.64	0.23	0.17	0.23
2016	Eigenvalues	317.45	31.75	13.07	1.16	0.65	0.22
	Percentage of Variance	87.13	8.72	3.59	0.32	0.18	0.06

Table 6 *Results of Modeling of PC1 Statistical Spatial Prediction for the time series of images between 1986 and 1991 in the Pao river basin*

Date of Image	SSPM	KriggingOrdinario
1986-12-17	CP1 SSPM	159.64*Nugget+31.758*J-Bessel(7602,5.7902)
	PRF	0.799731574082857 * x + 7.05960598625623
	ERF	-0.200268425931927 * x + 7.05960598676827
	SERF	-0.0154675752092125 * x + 0.54524241176202
	Samples	3209460
	Mean Error	-0.0019173166839584314
	Root-Mean-Square Error	5.1862243104401085
	Mean Standardized Error	-0.00014926537731710268
	Root-Mean-Square Standardized Error	0.40050630917911345
	Average Standard Error	12.947360217762062
1987-12-12	CP1 SSPM	0.097*Nugget+76.111*J-Bessel(64.405,2.0767)
	PRF	0.889478992125323 * x + 3.88654695824879
	ERF	-0.110521007872142 * x + 3.88654695815341
	SERF	-0.0160340988929681 * x + 0.563850296625761
	Samples	3209460
	Mean Error	0.0018465977454287514
	Root-Mean-Square Error	3.898472158233897
	Mean Standardized Error	0.00016780333774329005
	Root-Mean-Square Standardized Error	0.5636863951205011
	Average Standard Error	6.888670197418042
1988-04-02	CP1 SSPM	54.134*Nugget+326.36*J-Bessel(989.15,9.2224)
	PRF	0.902282369636342 * x + 4.61826614802535
	ERF	-0.0977176303647713 * x + 4.61826614808384
	SERF	-0.012921629881312 * x + 0.610679849129799
	Samples	3209460
	Mean Error	-0.0003050127444388146
	Root-Mean-Square Error	5.557555260279461
	Mean Standardized Error	-5.965826071557145e-005
	Root-Mean-Square Standardized Error	0.734312845440025
	Average Standard Error	7.560542716851552
1989-10-14	CP1 SSPM	84.714*Nugget+284.77*J-Bessel(1084.2,2.5598)
	PRF	0.901454202041896 * x + 4.23186554810007
	ERF	-0.0985457979590722 * x + 4.23186554816133
	SERF	-0.0104366787658701 * x + 0.448179093198231
	Samples	3209460
	Mean Error	-0.0007626455418015807
	Root-Mean-Square Error	5.108037627915864
	Mean Standardized Error	-9.005058363326744e-005
	Root-Mean-Square Standardized Error	0.5406895220799085
	Average Standard Error	9.441980564390827
1990-01-10	CP1 SSPM	93.06*Nugget+26.172*J-Bessel(10285,10)
	PRF	0.703229399531795 * x + 10.7993326061133
	ERF	-0.296770600460002 * x + 10.7993326058145
	SERF	-0.0300190349161297 * x + 1.09238418157416
	Samples	3209460
	Mean Error	0.0002135973177622011
	Root-Mean-Square Error	5.28894953218514
	Mean Standardized Error	1.9137466452028658e-005
	Root-Mean-Square Standardized Error	0.5349612674187941

	Average Standard Error	9.885314796283724
1991-03-18	CP1 SSPM	50.08*Nugget+38.762*J-Bessel(930.12,10)
	PRF	0.78781101578049 * x + 8.44603370464268
	ERF	-0.212188984223356 * x + 8.44603370479447
	SERF	-0.0292411234294779 * x + 1.16392340098242
	Samples	3209460
	Mean Error	0.00041439428085523203
	Root-Mean-Square Error	4.787403770202878
	Mean Standardized Error	4.967220533336505e-005
	Root-Mean-Square Standardized Error	0.6595792663863833
	Average Standard Error	7.255330994915141

SSPM: Statistical Spatial Prediction Model, PRF: Predicted Regression function, ERF: Error Regression Function, SERF: Standardized Error Regression Function, PE: Prediction Errors.

Table 7 *Results of Modeling of PC1 Statistical Spatial Prediction for the time series of images between 1996 and 2003 in the Pao river basin*

Image Date	SSPM	KriggingOrdinario
1996-10-25	CP1 SSPM	205.97*Nugget+623.24*J-Bessel(1048.7,10)
	PRF	0.911847018491454 * x + 3.0772456719974
	ERF	-0.0881529814835731 * x + 3.07724567111303
	SERF	-0.00598624997099158 * x + 0.208962582046893
	Samples	3209460
	Mean Error	0.0002361411944831531
	Root-Mean-Square Error	6.952142581022121
	Mean Standardized Error	9.040431070166409e-006
	Root-Mean-Square Standardized Error	0.47194407012537226
	Average Standard Error	14.7243092196546
1997-05-05	CP1 SSPM	310.33*Nugget+466.06*J-Bessel(2089.5,10)
	PRF	0.894066850677241 * x + 4.87510746067751
	ERF	-0.105933149328431 * x + 4.87510746093857
	SERF	-0.00586772965482358 * x + 0.270034219232626
	Samples	3209460
	Mean Error	0.000387580272136297
	Root-Mean-Square Error	7.420257109859033
	Mean Standardized Error	1.931519392532719e-005
	Root-Mean-Square Standardized Error	0.41097477765655654
	Average Standard Error	18.05260380725329
1998-02-01	CP1 SSPM	74.25*Nugget+19.209*J-Bessel(5725.8,1.6071)
	PRF	0.764681287942356 * x + 8.52765174704023
	ERF	-0.235318712063256 * x + 8.52765174724663
	SERF	-0.0266491954774068 * x + 0.965733444200238
	Samples	3209460
	Mean Error	0.0012559177124396325
	Root-Mean-Square Error	4.70088169444872
	Mean Standardized Error	0.0001391375112095437
	Root-Mean-Square Standardized Error	0.5323196031897652
	Average Standard Error	8.829911992963925
1999-01-19	CP1 SSPM	45.365*Nugget+30.447*J-Bessel(1561.4,10)
	PRF	0.696624976920017 * x + 10.7200708164001
	ERF	-0.303375023076431 * x + 10.7200708162761
	SERF	-0.0439452312244089 * x + 1.55284757948658
	Samples	3209460

	Mean Error	0.0007799062758078891
	Root-Mean-Square Error	4.81780373275036
	Mean Standardized Error	0.00010769952539223274
	Root-Mean-Square Standardized Error	0.6978087573357692
	Average Standard Error	6.903091750871226
2000-01-14	CP1 SSPM	54.377*Nugget+11.855*J-Bessel(21540,10)
	PRF	0.703252761472107 * x + 8.34425823397275
	ERF	-0.296747238526837 * x + 8.34425823394567
	SERF	-0.0392697378537949 * x + 1.10423559947758
	Samples	3209460
	Mean Error	0.0017249972254052496
	Root-Mean-Square Error	4.188480984250345
	Mean Standardized Error	0.000225049233233831
	Root-Mean-Square Standardized Error	0.5542426001813652
	Average Standard Error	7.556388965855685
2001-01-08	CP1 SSPM	59.823*Nugget+40.94*J-Bessel(1063.8,0.83536)
	PRF	0.774561438255423 * x + 7.9257530330345
	ERF	-0.225438561756292 * x + 7.92575303344383
	SERF	-0.0284352400150651 * x + 0.999705037515326
	Samples	3209460
	Mean Error	0.0007942935902049207
	Root-Mean-Square Error	4.832476870328396
	Mean Standardized Error	9.417744764782963e-005
	Root-Mean-Square Standardized Error	0.609399764859904
	Average Standard Error	7.928230627386897
2002-02-20	CP1 SSPM	32.763*Nugget+31.259*J-Bessel(768.9,10)
	PRF	0.810445926499447 * x + 5.55054837558971
	ERF	-0.189554073512134 * x + 5.55054837593189
	SERF	-0.0322715057494078 * x + 0.944972302359014
	Samples	3209460
	Mean Error	0.0005157982606197191
	Root-Mean-Square Error	4.162259278136349
	Mean Standardized Error	7.475205091843644e-005
	Root-Mean-Square Standardized Error	0.708470044071738
	Average Standard Error	5.87289745166136
2003-01-22	CP1 SSPM	33.077*Nugget+22.274*J-Bessel(1756.5,10)
	PRF	0.810141456241153 * x + 4.94681418534353
	ERF	-0.189858543761731 * x + 4.9468141854209
	SERF	-0.0322106970066574 * x + 0.839252201078166
	Samples	3209460
	Mean Error	0.0008555654354083932
	Root-Mean-Square Error	3.7662111254077453
	Mean Standardized Error	0.00014082041175700772
	Root-Mean-Square Standardized Error	0.6388667298074561
	Average Standard Error	5.894237351562172

SSPM: Statistical Spatial Prediction Model, PRF: Predicted Regression function, ERF: Error Regression Function, SERF: Standardized Error Regression Function, PE: Prediction Errors.

Table 8 *Results of Modeling of PC1 Statistical Spatial Prediction for the time series of images between 2015 and 2016 in the Pao river basin*

Image Date	SSPM	KriggingOrdinario
2015-03-04	CP1 SSPM	114.17*Nugget+29.926*J-Bessel(8543.9,10)
	PRF	0.82162642122063 * x + 6.34632257940418
	ERF	-0.178373578777378 * x + 6.34632257933382
	SERF	-0.0162896615727218 * x + 0.579566435521559
	Samples	3209460
	Mean Error	-0.00083668886522783
	Root-Mean-Square Error	4.914518766730799
	Mean Standardized Error	-7.853671650026577e-005
	Root-Mean-Square Standardized Error	0.44874908207113473
	Average Standard Error	10.949393610905199
2016-01-18	CP1 SSPM	29.446*Nugget+37.468*J-Bessel(698.43,3.2634)
	PRF	0.708783902685329 * x + 9.73369182020995
	ERF	-0.291216097316587 * x + 9.7336918202749
	SERF	-0.0522984189997559 * x + 1.74803305891607
	Samples	3209460
	Mean Error	0.00034861763405749337
	Root-Mean-Square Error	4.558879876022711
	Mean Standardized Error	4.642839411160511e-005
	Root-Mean-Square Standardized Error	0.8185263904213044
	Average Standard Error	5.568073894072198

SSPM: Statistical Spatial Prediction Model, PRF: Predicted Regression function, ERF: Error Regression Function, SERF: Standardized Error Regression Function, PE: Prediction Errors.

Table 9 *Forecasting of PC1 SSPM Coefficients based on the time series between 1986 and 1991*

	Coefficient a	b	c	d
(A)	ARIMA(1,0,0) with constant	ARIMA(1,0,0) with constant	ARIMA(1,0,0) with constant	ARIMA(1,0,0) with constant
(B)	Linear trend = 13597.7 + -6.80114 t	Linear trend = 9015.67 - 4.4682 t	Linear trend = 151355. - 74.359 t	Linear trend = -2161.21 + 1.09018 t
(C)	Simple exponential smoothing with alpha = 0.0775	Simple exponential smoothing with alpha = 0.1288	Simple exponential smoothing with alpha = 0.1098	Simple exponential smoothing with alpha = 0.1783
(D)	Brown's linear exp. smoothing with alpha = 0.038	Brown's linear exp. smoothing with alpha = 0.0605	Brown's linear exp. smoothing with alpha = 0.0536	Brown's linear exp. smoothing with alpha = 0.0691
(E)	Brown's quadratic exp. smoothing with alpha = 0.0251	Brown's quadratic exp. smoothing with alpha = 0.0392	Brown's quadratic exp. smoothing with alpha = 0.0352	Brown's quadratic exp. smoothing with alpha = 0.0428

Table 10 *Forecasting of PC1 SSPM Coefficients based on the time series between 1996 and 2003*

	Coefficient a	b	c	d
(A)	ARIMA(1,0,0) with constant	ARIMA(1,0,0) with constant	ARIMA(1,0,0) with constant	ARIMA(1,0,0) with constant
(B)	Linear trend = 62761.4 + -31.3376 t	Linear trend = 150931 - 75.4067 t	Linear trend = -98879.9 + 51.675 t	Linear trend = 62.9158 - 0.0275621 t
(C)	Simple exponential smoothing with alpha = 0.6694	Simple exponential smoothing with alpha = 0.9999	Simple exponential smoothing with alpha = 0.9999	Simple exponential smoothing with alpha = 0.9999
(D)	Brown's linear exp. smoothing with alpha = 0.0468	Brown's linear exp. smoothing with alpha = 0.0459	Brown's linear exp. smoothing with alpha = 0.0277	Brown's linear exp. smoothing with alpha = 0.0416
(E)	Brown's quadratic exp. smoothing with alpha = 0.0304	Brown's quadratic exp. smoothing with alpha = 0.0273	Brown's linear exp. smoothing with alpha = 0.0279	Brown's quadratic exp. smoothing with alpha = 0.0268

Table 11 *Error statistics by fitting the forecasting models to the CP1 SSPM coefficients based on the time series between 1986 and 1991*

Model	a			b			c			d		
	RMSE	MAE	ME	RMSE	MAE	ME	RMSE	MAE	ME	RMSE	MAE	ME
(A)	43.0168	26.4774	3.2464	149.069	104.798	4.34991	4306.73	3113.61	189.467	3.84892	2.67851	-0.0371282
(B)	57.9756	37.7331	1.98952E-13	153.15	116.606	1.51582E-13	4829.95	3609.23	1.45519E-11	3.41457	2.49656	-1.4877E-14
(C)	57.0119	40.6444	10.2037	149.267	112.128	26.5401	4694.35	3529.3	947.312	4.01324	3.50042	-0.0152302
(D)	56.9325	40.6381	9.6481	148.588	113.471	22.6457	4664.11	3574.5	827.624	4.08045	3.56827	-0.140601
(E)	56.9077	40.632	9.48725	148.415	113.754	21.7463	4654.4	3586.65	793.324	4.10102	3.58426	-0.207678

RMSE = root mean squared error, MAE = mean absolute error, ME = mean error

Table 12 *Error statistics by fitting the forecasting models to the CP1 SSPM coefficients based on the time series between 1996 and 2003*

Model	a			b			c			d		
	RMSE	MAE	ME	RMSE	MAE	ME	RMSE	MAE	ME	RMSE	MAE	ME
(A)	71.3372	46.1758	-2.03837E-12	174.613	85.5275	-38.578	7411.07	4401.36	-18.0989	4.01972	2.94246	0.0740119
(B)	94.0695	58.6162	-33.1682	172.03	130.048	1.86873E-12	7652.26	4607.24	-2.55795E-12	4.39443	3.29204	5.66214E-15
(C)	108.886	87.5653	-4.02591	179.637	85.1992	-75.1262	11026.1	6322.22	88.396	6.6422	4.38938	-9.64675E-10
(D)	109.578	86.3727	-0.559163	259.724	207.967	-6.1749	7420.63	4123.25	1325.63	4.30965	3.07081	-0.707596
(E)	94.5702	64.261	-9.13959	260.766	204.837	2.75543	7420.49	4128.36	1317.94	4.30232	3.08073	-0.682335

RMSE = root mean squared error, MAE = mean absolute error, ME = mean error

Table 13 *Forecasting of PC1 SSPM Coefficients between 1992 and 2003 based on the time series between 1986 and 1991 from forecasting model identified as ARIMA(1,0,0)*

Period	a			b			c			d		
	Forecast	Lower 95.0% Limit	Upper 95.0% Limit	Forecast	Lower 95.0% Limit	Upper 95.0% Limit	Forecast	Lower 95.0% Limit	Upper 95.0% Limit	Forecast	Lower 95.0% Limit	Upper 95.0% Limit
1992	81.6504	-41.8461	205.147	100.212	-314.743	515.167	4621.89	-7536.42	16780.2	5.14162	-5.54938	15.8326
1993	55.0623	-106.396	216.521	115.957	-312.403	544.318	2761.6	-10853.1	16376.3	6.99896	-4.44665	18.4446
1994	77.4543	-106.234	261.142	119.992	-309.234	549.218	3699.0	-10261.3	17659.3	6.28891	-5.26286	17.8407
1995	58.5962	-139.351	256.543	121.026	-308.257	550.308	3226.64	-10820.1	17273.4	6.56036	-5.00685	18.1276
1996	74.4782	-132.99	281.946	121.29	-307.996	550.577	3464.67	-10603.9	17533.2	6.45658	-5.11288	18.026
1997	61.1026	-152.861	275.067	121.358	-307.929	550.645	3344.72	-10729.4	17418.9	6.49626	-5.07353	18.066
1998	72.3673	-146.087	290.822	121.376	-307.911	550.663	3405.16	-10670.4	17480.7	6.48109	-5.08875	18.0509
1999	62.8804	-158.704	284.464	121.38	-307.907	550.667	3374.71	-10701.2	17450.6	6.48689	-5.08296	18.0567
2000	70.8701	-152.907	294.648	121.381	-307.906	550.668	3390.05	-10685.9	17466.0	6.48467	-5.08517	18.0545
2001	64.1413	-161.179	289.461	121.382	-307.905	550.669	3382.32	-10693.7	17458.3	6.48552	-5.08433	18.0554
2002	69.8082	-156.6	296.216	121.382	-307.905	550.669	3386.22	-10689.8	17462.2	6.48519	-5.08465	18.055
2003	65.0356	-162.141	292.212	121.382	-307.905	550.669	3384.25	-10691.8	17460.3	6.48532	-5.08453	18.0552
2004	69.055	-158.665	296.775	121.382	-307.905	550.669	3384.75	-10691.3	17460.8	6.48529	-5.08456	18.0551
2005	65.6699	-162.435	293.774	121.382	-307.905	550.669	3385.0	-10691.0	17461.0	6.48528	-5.08456	18.0551
2006	68.5208	-159.856	296.898	121.382	-307.905	550.669	3384.87	-10691.1	17460.9	6.48528	-5.08456	18.0551
2007	66.1199	-162.45	294.69	121.382	-307.905	550.669	3384.93	-10691.1	17460.9	6.48528	-5.08456	18.0551
2008	68.1419	-160.565	296.849	121.382	-307.905	550.669	3384.9	-10691.1	17460.9	6.48528	-5.08456	18.0551
2009	66.439	-162.365	295.243	121.382	-307.905	550.669	3384.92	-10691.1	17460.9	6.48528	-5.08456	18.0551
2010	67.8731	-160.999	296.746	121.382	-307.905	550.669	3384.91	-10691.1	17460.9	6.48528	-5.08456	18.0551
2011	66.6653	-162.256	295.587	121.382	-307.905	550.669	3384.91	-10691.1	17460.9	6.48528	-5.08456	18.0551
2012	67.6825	-161.273	296.638	121.382	-307.905	550.669	3384.91	-10691.1	17460.9	6.48528	-5.08456	18.0551
2013	66.8258	-162.155	295.806	121.382	-307.905	550.669	3384.91	-10691.1	17460.9	6.48528	-5.08456	18.0551
2014	67.5473	-161.45	296.545	121.382	-307.905	550.669	3384.91	-10691.1	17460.9	6.48528	-5.08456	18.0551
2015	66.9397	-162.07	295.95	121.382	-307.905	550.669	3384.91	-10691.1	17460.9	6.48528	-5.08456	18.0551
2016	67.4514	-161.567	296.47	121.382	-307.905	550.669	3384.91	-10691.1	17460.9	6.48528	-5.08456	18.0551
2017	67.0205	-162.005	296.046	121.382	-307.905	550.669	3384.91	-10691.1	17460.9	6.48528	-5.08456	18.0551
2018	67.3834	-161.646	296.413	121.382	-307.905	550.669	3384.91	-10691.1	17460.9	6.48528	-5.08456	18.0551
2019	67.0777	-161.955	296.11	121.382	-307.905	550.669	3384.91	-10691.1	17460.9	6.48528	-5.08456	18.0551
2020	67.3352	-161.7	296.37	121.382	-307.905	550.669	3384.75	-10691.3	17460.8	6.48529	-5.08456	18.0551
2021	67.1184	-161.918	296.155	121.382	-307.905	550.669	3384.91	-10691.1	17460.9	6.48528	-5.08456	18.0551
2022	67.3009	-161.737	296.338	121.382	-307.905	550.669	3384.91	-10691.1	17460.9	6.48528	-5.08456	18.0551

2023	67.1472	-161.891	296.185	121.382	-307.905	550.669	3384.91	-10691.1	17460.9	6.48528	-5.08456	18.0551
2024	67.2767	-161.762	296.316	121.382	-307.905	550.669	3384.91	-10691.1	17460.9	6.48528	-5.08456	18.0551
2025	67.1676	-161.872	296.207	121.382	-307.905	550.669	3384.91	-10691.1	17460.9	6.48528	-5.08456	18.0551
2026	67.2595	-161.78	296.299	121.382	-307.905	550.669	3384.91	-10691.1	17460.9	6.48528	-5.08456	18.0551
2027	67.1821	-161.858	296.222	121.382	-307.905	550.669	3384.91	-10691.1	17460.9	6.48528	-5.08456	18.0551
2028	67.2473	-161.793	296.287	121.382	-307.905	550.669	3384.91	-10691.1	17460.9	6.48528	-5.08456	18.0551
2029	67.1924	-161.848	296.232	121.382	-307.905	550.669	3384.91	-10691.1	17460.9	6.48528	-5.08456	18.0551
2030	67.2386	-161.801	296.279	121.382	-307.905	550.669	3384.75	-10691.3	17460.8	6.48529	-5.08456	18.0551

Table 14 *Forecasting of PC1 SSPM Coefficients between 2004 and 2020 based on the time series between 1996 and 2003 from forecasting model identified as model Brown's linear exponential smoothing with alpha = 0.4099*

Period	a			b			c			d		
	Forecast	Lower 95.0% Limit	Upper 95.0% Limit	Forecast	Lower 95.0% Limit	Upper 95.0% Limit	Forecast	Lower 95.0% Limit	Upper 95.0% Limit	Forecast	Lower 95.0% Limit	Upper 95.0% Limit
2004	94.521	-105.138	294.18	130.136	-345.562	605.833	3513.14	-10091.5	17117.7	8.15412	0.253187	16.0551
2005	95.7068	-104.989	296.402	131.933	-345.369	609.235	3534.9	-10090.9	17160.7	8.12227	0.194037	16.0505
2006	96.8925	-104.887	298.672	133.73	-345.237	612.698	3556.66	-10090.8	17204.1	8.09042	0.133839	16.047
2007	98.0782	-104.833	300.989	135.528	-345.167	616.222	3578.42	-10091.3	17248.2	8.05857	0.0725815	16.0446
2008	99.2639	-104.828	303.356	137.325	-345.159	619.808	3600.19	-10092.4	17292.8	8.02672	0.0102521	16.0432
2009	100.45	-104.873	305.772	139.122	-345.214	623.458	3621.95	-10094.1	17338.0	7.99487	-0.0531601	16.0429
2010	101.635	-104.967	308.238	140.919	-345.332	627.171	3643.71	-10096.4	17383.8	7.96302	-0.117665	16.0437
2011	102.821	-105.111	310.753	142.717	-345.514	630.948	3665.48	-10099.2	17430.2	7.93117	-0.183274	16.0456
2012	104.007	-105.306	313.32	144.514	-345.762	634.79	3687.24	-10102.7	17477.1	7.89931	-0.249995	16.0486
2013	105.193	-105.551	315.937	146.311	-346.074	638.696	3709.0	-10106.7	17524.7	7.86746	-0.317836	16.0528
2014	106.378	-105.848	318.605	148.108	-346.452	642.669	3730.77	-10111.3	17572.9	7.83561	-0.386807	16.058
2015	107.564	-106.196	321.324	149.906	-346.896	646.708	3752.53	-10116.6	17621.6	7.80376	-0.456914	16.0644
2016	108.75	-106.595	324.094	151.703	-347.407	650.813	3774.29	-10122.4	17671.0	7.77191	-0.528164	16.072
2017	109.935	-107.045	326.916	153.5	-347.984	654.985	3796.05	-10128.9	17721.0	7.74006	-0.600563	16.0807
2018	107.975	-107.485	323.434	155.498	-348.582	659.579	3817.82	-10136.0	17771.6	7.72766	-0.642451	16.0978
2019	109.069	-107.835	325.973	157.301	-349.303	663.905	3839.58	-10143.7	17822.8	7.69631	-0.715472	16.1081
2020	110.164	-108.226	328.553	159.103	-350.092	668.299	3861.34	-10152.0	17874.7	7.66497	-0.789619	16.1196
2021	112.276	-108.743	333.295	167.919	-350.373	686.211	3870.26	-10167.3	17907.8	7.61266	-0.901758	16.1271
2022	113.397	-109.279	336.073	169.947	-351.741	691.636	3891.78	-10176.6	17960.2	7.58081	-0.979977	16.1416
2023	114.518	-109.86	338.896	171.975	-353.201	697.151	3913.3	-10186.5	18013.2	7.54895	-1.05937	16.1573
2024	115.639	-110.484	341.762	174.004	-354.752	702.759	3934.82	-10197.1	18066.8	7.5171	-1.13994	16.1741
2025	116.76	-111.153	344.673	176.032	-356.394	708.458	3956.35	-10208.3	18121.0	7.48525	-1.22169	16.1922
2026	117.881	-111.865	347.628	178.06	-358.129	714.249	3977.87	-10220.2	18175.9	7.4534	-1.30462	16.2114
2027	119.002	-112.622	350.627	180.088	-359.954	720.131	3999.39	-10232.7	18231.5	7.42155	-1.38873	16.2318
2028	120.123	-113.422	353.669	182.116	-361.871	726.104	4020.91	-10245.8	18287.6	7.3897	-1.47402	16.2534
2029	121.245	-114.266	356.755	184.145	-363.879	732.169	4042.43	-10259.6	18344.5	7.35785	-1.56048	16.2762
2030	122.366	-115.154	359.885	186.173	-365.978	738.324	4063.95	-10274.0	18401.9	7.326	-1.64813	16.3001

Table 15 *Calibration of PC1 SSPM with forecasted coefficients between 1996 and 2003 based on the time series between 1986 and 1991; which will be used in the validation stage.*

Image Date	SSPM	KriggingOrdinario	Independent Variable
1996	CP1 SSPM	74.478*Nugget+121.29*J-Bessel(3464.7,6.4566))	PC1 Image in 1991
	PRF	0.782457400083391 * x + 8.66576413426161	
	ERF	-0.217542599920342 * x + 8.66576413440802	
	SERF	-0.0245960106431233 * x + 0.979778911923131	
	Samples	3209460	
	Mean Error	-0.001497892148731668	
	Root-Mean-Square Error	4.836050429299965	
	Mean Standardized Error	-0.00017234050107555393	
	Root-Mean-Square Standardized Error	0.5466944483203884	
	Average Standard Error	8.84396133470597	
1997	CP1 SSPM	61.103*Nugget+121.36*J-Bessel(3344.7,6.4963)	PC1 Image in 1991
	PRF	0.78249065167316 * x + 8.66449102403397	

	ERF	-0.217509348330553	*	x	+ 8.66449102417957	
	SERF	-0.0271500749218015	*	x	+ 1.08152656268913	
	Samples	3209460				
	Mean Error	-0.0014502284528388049				
	Root-Mean-Square Error	4.834793617851682				
	Mean Standardized Error	-0.00018454167290494				
	Root-Mean-Square Standardized Error	0.6034000737986222				
	Average Standard Error	8.010678795781427				
1998	CP1 SSPM	72.367*Nugget+121.38*J-Bessel(3405.2,6.4811)				PC1 Image in 1991
	PRF	0.782472094908954	*	x	+ 8.66522076979606	
	ERF	-0.217527905094886	*	x	+ 8.66522076994925	
	SERF	-0.0249510404101306	*	x	+ 0.993921693698665	
	Samples	3209460				
	Mean Error	-0.0014921951969875885				
	Root-Mean-Square Error	4.8357612779715415				
	Mean Standardized Error	-0.00017422035047323393				
	Root-Mean-Square Standardized Error	0.5545741662264446				
	Average Standard Error	8.717762664058569				
1999	CP1 SSPM	62.88*Nugget+121.38*J-Bessel(3374.7,6.4869)				PC1 Image in 1991
	PRF	0.782485698055638	*	x	+ 8.66467297542527	
	ERF	-0.217514301948082	*	x	+ 8.66467297557441	
	SERF	-0.0267635231075235	*	x	+ 1.06612641224482	
	Samples	3209460				
	Mean Error	-0.0014737771749448352				
	Root-Mean-Square Error	4.835009744341121				
	Mean Standardized Error	-0.00018474176363632915				
	Root-Mean-Square Standardized Error	0.5948387374561481				
	Average Standard Error	8.126353188324524				
2000	CP1 SSPM	70.87*Nugget+121.38*J-Bessel(3390.1,6.4847)				PC1 Image in 1991
	PRF	0.782473617235265	*	x	+ 8.66515200127705	
	ERF	-0.217526382768478	*	x	+ 8.66515200142597	
	SERF	-0.0252121603364036	*	x	+ 1.00432774922535	
	Samples	3209460				
	Mean Error	-0.0014882161367605 14				
	Root-Mean-Square Error	4.835628167509834				
	Mean Standardized Error	-0.00017561014169653277				
	Root-Mean-Square Standardized Error	0.5603845947289107				
	Average Standard Error	8.62712593246869				
2001	CP1 SSPM	64.141*Nugget+121.38*J-Bessel(3382.3,6.4855)				PC1 Image in 1991
	PRF	0.782485494414201	*	x	+ 8.66467662426456	
	ERF	-0.21751450558953	*	x	+ 8.66467662441265	
	SERF	-0.0264990951312986	*	x	+ 1.05559536437623	

	Samples	3209460				
	Mean Error	-0.0014731494647191735				
	Root-Mean-Square Error	4.8351287820392885				
	Mean Standardized Error	-0.00018282399848751105				
	Root-Mean-Square Standardized Error	0.5889789262324034				
	Average Standard Error	8.207412043022755				
2002	CP1 SSPM	69.808*Nugget+121.38*J-Bessel(3386.2,6.4852)				PC1 Image in 1991
	PRF	0.782472355473317	*	x	+ 8.66520140189453	
	ERF	-0.217527644530358	*	x	+ 8.6652014020402	
	SERF	-0.0254027991562895	*	x	+ 1.01192551726518	
	Samples	3209460				
	Mean Error	-0.001488079705035085				
	Root-Mean-Square Error	4.835551531112071				
	Mean Standardized Error	-0.0001769316167655006				
	Root-Mean-Square Standardized Error	0.5646208695700107				
	Average Standard Error	8.562257394661494				
2003	CP1 SSPM	65.036*Nugget+121.38*J-Bessel(3384.3,6.4853)				PC1 Image in 1991
	PRF	0.782486186389989	*	x	+ 8.66468110670922	
	ERF	-0.217513813613766	*	x	+ 8.66468110685723	
	SERF	-0.0263168048917327	*	x	+ 1.04833145569751	
	Samples	3209460				
	Mean Error	-0.0014735721905353844				
	Root-Mean-Square Error	4.835204726375911				
	Mean Standardized Error	-0.00018160361769975432				
	Root-Mean-Square Standardized Error	0.584925471074053				
	Average Standard Error	8.264422702639893				
2016	CP1 SSPM	67.451*Nugget+296.47*J-Bessel(3384.9,6.4853)				PC1 Image in 1991
	PRF	0.782850935623846	*	x	+ 8.64984198591374	
	ERF	-0.21714906437995	*	x	+ 8.64984198606454	
	SERF	-0.0257981582998008	*	x	+ 1.02765240164243	
	Samples	3209460				
	Mean Error	-0.0013296797742065646				
	Root-Mean-Square Error	4.829302987949121				
	Mean Standardized Error	-0.0001620197273095237				
	Root-Mean-Square Standardized Error	0.5735859258764888				
	Average Standard Error	8.417173183173139				

SSPM: Statistical Spatial Prediction Model, PRF: Predicted Regression function, ERF: Error Regression Function, SERF: Standardized Error Regression Function, PE: Prediction Errors, x: observed value

Table 16 *Calibration of PC1 SSPM with forecasted coefficients between 2015 and 2016 based on the time series between 1996 and 2003, which will be used in the validation stage.*

Image Date	SSPM	KriggingOrdinario	Independent Variable
2015-03-04	CP1 SSPM	106.94*Nugget+155.35*J-Bessel(3769.5,7.8181)	PC1 Image in 2003
	PRF	0.809963487240562 * x + 4.95130829635777	
	ERF	-0.190036512762404 * x + 4.95130829643601	
	SERF	-0.017932076069803 * x + 0.467209745767224	
	Samples	3209460	
	Mean Error	0.0008837443260897917	
	Root-Mean-Square Error	3.7707000884257074	
	Mean Standardized Error	8.131811541666571e-005	
	Root-Mean-Square Standardized Error	0.35576399222682814	
	Average Standard Error	10.597455237491586	
2016-01-18	CP1 SSPM	108.11*Nugget+157.31*J-Bessel(3791.7,7.7866)	PC1 Image in 2003
	PRF	0.809964799096486 * x + 4.95128369002492	
	ERF	-0.190035200906579 * x + 4.95128369010575	
	SERF	-0.0178352201504645 * x + 0.464685003551203	
	Samples	3209460	
	Mean Error	0.0008823213018557619	
	Root-Mean-Square Error	3.7707353943426187	
	Mean Standardized Error	8.075029911057093e-005	
	Root-Mean-Square Standardized Error	0.35384383543414616	
	Average Standard Error	10.65506565229091	

Table 17 *Validation of the forecasting of PC1 SSPM versus the observed PC1 between 1996 and 2003 based on the time series between 1986 and 1991*

Image Date	SSPM	Statistics	Independent Variable
1996	PRF	23.1465 + 0.423927*x	PC1 Image in 1991
	Samples	73	
	CC	0.652297	
	R^2	0.425492	
	$R^2_{adjusted}$	0.417512	
	SEE	33.1997	
	MAE	27.5367	
	DW	1.14484	
1997	PRF	47.0283 + 0.50922*x	PC1 Image in 1991
	Samples	84	
	CC	0.650279	
	R^2	0.422863	
	$R^2_{adjusted}$	0.415825	
	SEE	30.0122	
	MAE	24.507	
	DW	1.17082	
1998	PRF	30.7165 + 0.773589*x	PC1 Image in 1991
	Samples	54	

	CC	0.615856	
	R^2	0.379279	
	$R^2_{adjusted}$	0.367342	
	SEE	19.0444	
	MAE	15.5405	
	DW	1.22745	
1999	PRF	41.1855 + 0.836547*x	PC1 Image in 1991
	Samples	89	
	CC	0.613302	
	R^2	0.37614	
	$R^2_{adjusted}$	0.368969	
	SEE	24.8915	
	MAE	21.247	
	DW	1.08158	
2000	PRF	22.4994 + 0.881861*x	PC1 Image in 1991
	Samples	90	
	CC	0.629097	
	R^2	0.395763	
	$R^2_{adjusted}$	0.388897	
	SEE	14.8382	
	MAE	12.7754	
	DW	0.898675	
2001	PRF	26.8065 + 0.869967*x	PC1 Image in 1991
	Samples	173	
	CC	0.566345	
	R^2	0.320747	
	$R^2_{adjusted}$	0.316775	
	SEE	26.6568	
	MAE	22.2843	
	DW	0.913673	
2002	PRF	37.2925 + 0.794873*x	PC1 Image in 1991
	Samples	264	
	CC	0.645069	
	R^2	0.416114	
	$R^2_{adjusted}$	0.413886	
	SEE	31.7812	
	MAE	27.105	
	DW	0.892394	
2003	PRF	26.3699 + 0.820973*x	PC1 Image in 1991
	Samples	109	
	CC	0.628676	
	R^2	0.395234	
	$R^2_{adjusted}$	0.389582	
	SEE	19.3724	
	MAE	16.6821	
	DW	0.938925	

PRF: Predicted Regression function, CC: Correlation Coefficient, R-squared: Determination Coefficient, $R^2_{adjusted}$: R-squared (adjusted), SEE: Standard Error of Estimation, MAE: Mean absolute error, DWs: Durbin-Watson statistic, x: observed value

Table 18 *Validation of the forecasting of PC1 SSPM versus the observed PC1 between 2015 and 2016 based on the time series between 1996 and 2003*

Image Date	SSPM	Statistics	Independent Variable
2015-03-04	PRF	27.4301 + 0.377642*x	CP1 Image in 1991
	Samples	361	
	CC	0.601136	
	R^2	36.1364	
	$R^2_{adjusted}$	35.9585	
	SEE	2.81384	
	MAE	2.11622	
	DW	1.42581	
2016-01-18	PRF	8.02645 + 0.422091*x	CP1 Image in 1991
	Samples	241	
	CC	0.547798	
	R^2	0.300083	
	$R^2_{adjusted}$	0.297154	
	SEE	2.90821	
	MAE	1.86529	
	DW	1.25292	

PRF: Predicted Regression function, CC: Correlation Coefficient, R-squared: Determination Coefficient, $R^2_{adjusted}$: R-squared (adjusted), SEE: Standard Error of Estimation, MAE: Mean absolute error, DWs: Durbin-Watson statistic, x: observed value

Table 19 *Calibration of PC1 SSPM for 2020 and 2030 with forecasted coefficients based on the time series between 1986 and 1991.*

Image Date	SSPM	KriggingOrdinario	Independent Variable
2020	CP1 SSPM	67.335*Nugget+121.38*J-Bessel(3384.8,6.4853)	PC1 Image in 1991
	PRF	0.782482497946622 * x + 8.66482580355468	
	ERF	-0.217517502057148 * x + 8.66482580370286	
	SERF	-0.0258635513022785 * x + 1.03028148988674	
	Samples	3209460	
	Mean Error	-0.001485463979409483	
	Root-Mean-Square Error	4.835357224567999	
	Mean Standardized Error	-0.000179863724460417	
	Root-Mean-Square Standardized Error	0.5748706897260144	
	Average Standard Error	8.409246666599419	
2030	CP1 SSPM	67.239*Nugget+121.38*J-Bessel(3384.8,6.4853)	PC1 Image in 1991
	PRF	0.782482635336724 * x + 8.66481780303473	
	ERF	-0.21751736466703 * x + 8.66481780318602	
	SERF	-0.0258820754738057 * x + 1.03101973857555	
	Samples	3209460	
	Mean Error	-0.0014852792995607186	
	Root-Mean-Square Error	4.835350380505459	
	Mean Standardized Error	-0.0001799718288230623	
	Root-Mean-Square Standardized Error	0.5752826014564657	
	Average Standard Error	8.403213221050384	

Table 20 *Calibration of PC1 SSPM for 2020 and 2030 with forecasted coefficients based on the time series between 1996 and 2003.*

Image Date	SSPM	KriggingOrdinario	Independent Variable
2020	CP1 SSPM	110.16*Nugget+159.1*J-Bessel(3861.3,7.665)	PC1 Image in 2003
	PRF	0.812623853936476 * x + 4.88183978346219	
	ERF	-0.187376146066429 * x + 4.88183978353553	
	SERF	-0.0174215684751477 * x + 0.453896626000269	
	Samples	3209460	
	Mean Error	0.0005492010950066949	
	Root-Mean-Square Error	3.744097772584058	
	Mean Standardized Error	4.898137496795628e-005	
	Root-Mean-Square Standardized Error	0.3480647978379873	
	Average Standard Error	10.75548056956617	
2030	CP1 SSPM	122.37*Nugget+186.17*J-Bessel(4063.9,7.326)	PC1 Image in 2003
	PRF	0.812621759964613 * x + 4.88189698850629	
	ERF	-0.187378240038252 * x + 4.88189698858003	
	SERF	-0.0165303975484998 * x + 0.430678392744302	
	Samples	3209460	
	Mean Error	0.0005496892571118923	
	Root-Mean-Square Error	3.744121163068481	
	Mean Standardized Error	4.653493745137874e-005	
	Root-Mean-Square Standardized Error	0.33025772645859125	
	Average Standard Error	11.335484639185395	

Table 21 *Results of the principal components transformation method expressed by the difference of the principal component No. 1 based on bitemporal reflectance images as a proportion of Change / No Change areas in the Pao river basin from 1986 to 2016; using the forecasted PC1 2016 from time series between 1986 and 1991. The parameters are: C: Change, NC: No Change, PAR: Percentage Area Ratio.*

BitemporalImages	1986-2016	1990-2016	2000-2016	2015-2016
PAR: C	4.94	7.91	8.83	5.85
PAR: NC	95.05	92.08	91.17	94.14

Table 22 *Results of the principal components transformation method expressed by the difference of the principal component No. 1 based on bitemporal reflectance images as a proportion of Change / No Change areas in the Pao river basin from 1986 to 2016; using the forecasted PC1 2016 from time series between 1996 and 2003. The parameters are: C: Change, NC: No Change, PAR: Percentage Area Ratio.*

BitemporalImages	1986-2016	1990-2016	2000-2016	2015-2016
PAR: C	4.66	7.83	7.65	4.71
PAR: NC	95.33	92.16	92.34	95.28

Table 23 *Results of the principal components transformation method expressed by the difference of the PC1 based on bitemporal reflectance images as a proportion of Change / No Change areas in the Pao river basin from 1986-2016; using the original PC1 2016. The parameters are: C: Change, NC: No Change, PAR: Percentage Area Ratio.*

BitemporalImages	1986-2016	1990-2016	2000-2016	2015-2016
PAR: C	5.01	7.05	5.13	3.98
PAR: NC	94.9	92.94	94.86	96.01

Table 24 *Results of the difference method of bitemporal reflectance images expressed by the proportion of Change / No Change areas in the Pao river basin from 1986-2016. The parameters are: C: Change, NC: No Change, PAR: Percentage Area Ratio.*

BitemporalImages	1986-2016	1990-2016	2000-2016	2015-2016
PAR: C	6.55	8.99	6.49	5.46
PAR: NC	93.45	91.01	93.51	94.54

Table 25 *Results of the method of the ratio of the reflectance images bitemporal expressed by the ratio of areas of change / no change in the maps obtained in the basin of the Pao River from 1986-2016. The parameters are: C: Change, NC: No Change, PAR: Percent Area Ratio.*

BitemporalImages	1986-2016	1990-2016	2000-2016	2015-2016
PAR: C	2.64	0.71	0.89	0.86
PAR: NC	97.36	99.29	99.11	99.14

Table 26 *Results of forecasted difference CP1 image being the forecasted CP1 based on the time series between 1986 and 1991, a) 2020-2016, b) 2030-2016*

BitemporalImages	2020-2016	2030-2016
PAR: C	5.54	8.14
PAR: NC	94.45	91.85

Table 27 *Results of forecasted difference CP1 image being the forecasted CP1 based on the time series between 1986 and 1991, a) 2020-2016, b) 2030-2016*

BitemporalImages	2020-2016	2030-2016
PAR: C	5.52	8.24
PAR: NC	94.48	91.75

Table 28 *Comparing of forecasting methods of LULC change detection*

References	**Prediction Method**	**Type of Model**	**Observed Images/Photography/ Time Series**	**Satellite/Photography**	**Observed image for validation**	**Future scenarios**
Pijanowski et al., (2002)	Neural Network	Multi-Layer Perceptron (MPL)	1980	Aerial photography	-	2010, 2020
Jianping et al., (2005)	Markovian chain analysis		1989, 2001	Landsat Thematic Mapper		1999, 2003
Yin et al., (2007)	Markovian chain analysis		2004, 2005	QuickBird, IKONOS, SPOT-5		2006
Hadi et al., (2014)	Markovian chain analysis		2000, 2010	Landsat Thematic Mapper	2010	2030
Mishra et al., (2014)	Neural Network	Multi-Layer Perceptron (MPL)	1988, 2010	Landsat Thematic Mapper	-	2025, 2035
Kumar et al., (2014)	Markovian chain		1998, 2006, 2009	Indian Remote Sensing Satellite	2009	2022

	analysis			(IRS)		
Han et al., (2015)	Markovian chain analysis		1985, 2000, 2010	Landsat Thematic Mapper	2010	2020
Padonou et al (2017)	Markovian chain analysis		1975, 1990, 2010	Landsat Multispectral Scanner, Landsat Thematic Mapper, Landsat Enhanced Thematic Mapper plus	1990, 2010	2050
This Study	Statistical Spatial Prediction Model / Forecasting Model	J-Bessel/ AutoRegressive, Integrated, Moving Average	1986,1987,1988,1989, 1990,1991	Landsat Thematic Mapper, Landsat Enhanced Thematic Mapper plus, Landsat Operational Land Imager	1996,1997,1998, 1999,2000, 2001, 2002, 2003, 2015, 2016	2020, 2030
	Statistical Spatial Prediction Model / Forecasting Model	J-Bessel / Brown's linear exponential smoothing	1996,1997,1998,1999, 2000, 2001, 2002, 2003	Landsat Thematic Mapper, Landsat Enhanced Thematic Mapper plus, Landsat Operational Land Imager	2015, 2016	2020, 2030
			2015, 2016	Landsat Operational Land Imager	2015, 2016	